Regd. No. C-3911

VOL. 35 **INDIAN JOURNAL OF PHYSICS** No. 8

(Published in collaboration with the Indian Physical Society)

AND

VOL. 44 **PROCEEDINGS** No. 8

OF THE

INDIAN ASSOCIATION FOR THE CULTIVATION OF SCIENCE

AUGUST 1961

PUBLISHED BY THE
INDIAN ASSOCIATION FOR THE CULTIVATION OF SCIENCE
JADAVPUR, CALCUTTA 32

Annual Subscription—
Inland Rs. 25.00
Foreign £ 2-10-0 or $ 7.00

NOTICE
TO INTENDING AUTHORS

1. Manuscripts for publication should be sent to the Assistant Editor, Indian Journal of Physics, Jadavpur, Calcutta-32.

2. The manuscripts submitted must be type-written with double space on thick foolscap paper with sufficient margin on the left and at the top. The original copy, and not the carbon copy, should be submitted. Each paper must contain an Abstract at the beginning.

3. All References should be given in the text by quoting the surname of the author, followed by year of publication, *e.g.*, (Roy, 1958). The full Reference should be given in a list at the end, arranged alphabatically, as follows; Mazumder, M. 1959, *Ind. J. Phys.*, **33**, 346.

4. Line diagrams should be drawn on white Bristol board or tracing paper with black Indian ink, and letters and numbers inside the diagrams should be written neatly in capital type with Indian ink. The size of the diagrams submitted and the lettering inside should be large enough so that it is legible after reduction to one-third the original size. A simple style of lettering such as gothic, with its uniform line width and no serifs should be used, *e.g.*,

A·B·E·F·G·M·P·T·W·

5. Photographs submitted for publication should be printed on glossy paper with somewhat more contrast than that desired in the reproduction.

6. Captions to all figures should be typed in a separate sheet and attached at the end of the paper.

7. The mathematical expressions should be written carefully by hand. Care should be taken to distinguish between capital and small letters and superscripts and subscripts. Repetition of a complex expression should be avoided by representing it by a symbol. Greek letters and unusual symbols should be identified in the margin. Fractional exponents should be used instead of root signs.

42

WING OF THE RAYLEIGH LINE RECORDED WITH A SELF-RECORDING GRATING SPECTROPHOTOMETER

S. C. SIRKAR, S. B. ROY AND D. K. GHOSH

OPTICS DEPARTMENT,

INDIAN ASSOCIATION FOR THE CULTIVATION OF SCIENCE, CALCUTTA-32

(*Received March* 29, 1961)

ABSTRACT. A self-recording spectrophotometer has been constructed using a Bausch and Lomb plane grating with Ebert mounting, a thirteen-dynode photomultiplier, a D.C. amplifier and a Honeywell-Brown pen recorder. The resolution is found to be much higher than that given by the commercial recording spectrophotometers in which prisms are used as the dispersing system.

The wing of the Rayleigh line due to benzene at different temperatures and that due to liquid oxygen have been studied with this instrument. Benzene at 5°C shows two broad maxima in the wing which disappear when the liquid is heated to 75°C. Liquid oxygen shows a feeble wing with inflections about 38, 49 and 60 cm^{-1} away from the Rayleigh line. These results have been discussed.

INTRODUCTION

The use of plane grating with Ebert mounting (Ebert, 1889) as the dispersing system in a recording monochromator was discussed recently by Fastie (1952) who constructed such a monochromator with a resolving power of about 91000 in the first order. Besides the high resolving power the monochromator has also high light gathering power. In this respect such a monochromator is better than most of the commercial recording spectrophotometers in which prisms are used as the dispersing system. A recording spectrophotometer with high resolving power has another advantage which is not possessed by spectrographs having high resolving power. For studying the relative intensity of a weak satellite or a feeble wing close to an intense line the photographic method is quite unsuitable, because the exposure necessary to record the weak satellite makes the stronger line overexposed and scattering in the grains of the emulsion makes the width of the line much larger than its actual width produced by the dispersing system. Therefore, the photographic method is unsuitable for the study of distribution of intensity in the wing of the Rayleigh line. As the true distribution of intensity in the wing might throw some light on the structure of the liquid a programme was undertaken to study it with the help of a self-recording grating spectrophotometer and an attempt was made to construct a spectrophotometer similar to the monochromator constructed by Fastie (1952). The performance of such a spectrophotometer constructed in the laboratory and also some preliminary

results of investigations on the distribution of intensity in the wing of the Rayleigh line have been discussed in the present paper.

DESCRIPTION OF THE SPECTROPHOTOMETER

A Bausch and Lomb plane grating of dimensions 65 mm × 76 mm with 2160 grooves per mm and blaze angle of 40°23′ was used as the dispersing system. A schlieren mirror having a radius of curvature 150 cm and aperture about 20 cm was used both for collimating the incident beam and focusing the diffracted beam on the exit slit. The mounting is symmetrical, the plane of the grating is vertical and the scanning arrangement is similar to that in Fastie's monochromator. The reversible D.C. motor used for the scanning is, however, run by a stabilised voltage.

A 6256 photomultiplier tube supplied by E.M.I. Research Laboratories of England is used as the detector. The tube is mounted coaxially in a horizontal brass cylinder surrounded by a spiral of copper tubing through which alcohol cooled by liquid oxygen can be circulated to cool the photomultiplier tube. The window of the brass cylinder is provided with an annular electric heater to prevent condensation of moisture on the window of the photomultiplier tube. The maximum voltage applied to each dynode is about 155 V. A voltage stabliser purchased from Hungary and capable of supplying 3000 volts is used to supply the voltages to the dynodes. The electron current from the anode can flow

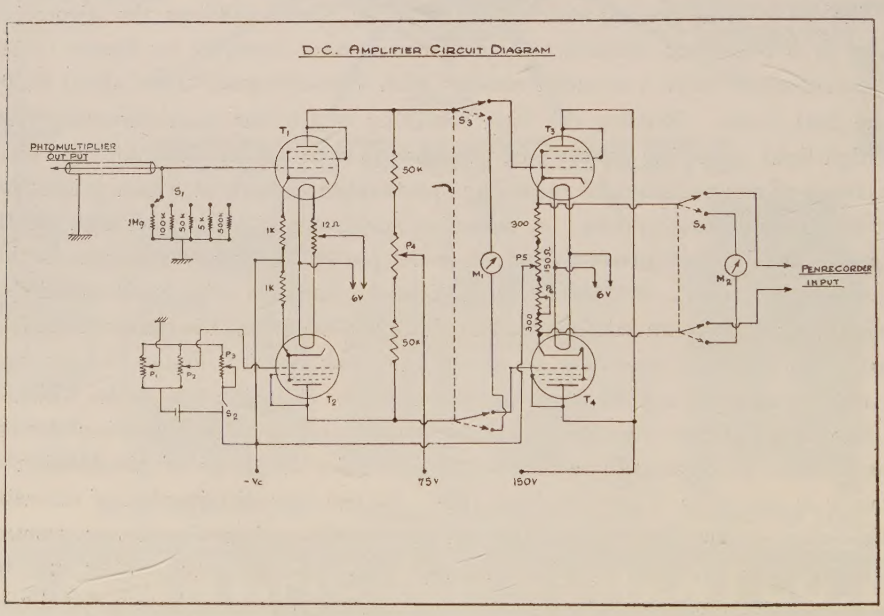

Fig. 1. Circuit diagram of D.C. amplifier.

through any one of the resistances of values 10K, 40K, 100K and 1 Megohm depending on the sensitivity required.

The output voltage of the photomultiplier tube is amplified by a D.C. amplifier designed on the principles of the circuit used by Chien and Bender (1947). The circuit had, however, to be modified in order to make it suitable for use with a Honeywell and Brown pen recorder. It was found initially that when the potential-drop across a high resistance was used to drive the pen recorder the pen became sluggish during its return sweep, broadening thereby the base of the peak due to any spectral line. So, the output of the balanced-bridge D.C. amplifier was fed to two cathode followers in balanced condition to reduce the effective resistance. The circuit diagram is given in Fig. 1. A photograph of the whole assembly is reproduced in Fig. 2.

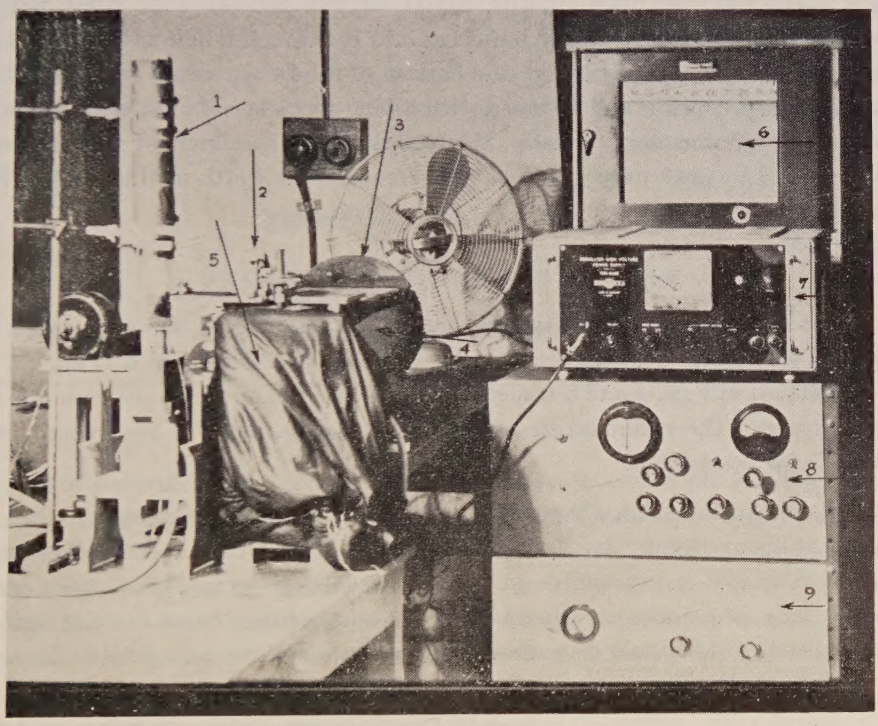

Fig. 2. Photograph of the recording spectrophotometer 1—Unsilvered [Dewar] flask of Pyrex glass, 2—Gear system for turning the grating, 3—Schilieren concave mirror, 4—All-metal body of the spectrograph, 5—Photomultiplier mount covered with black cloth, 6—Pen recorder, 7—High voltage stabilizer, 8—D. C. amplifier, 9—Stabilizer for D. C. amplifier.

EXPERIMENTAL

In order to study the wing of the Rayleigh line due to benzene a horizontal Raman tube of diameter about 25 mm provided with a jacket was used. Ice-cold water was first circulated through the jacket and the temperature of the

liquid was thereby brought down to 5°C. After recording the wing accompanying the Rayleigh line 4047A of Hg, the liquid was heated to 75°C by circulating hot water through the jacket and the wing in the same region was again recorded. Several records were taken for each of the temperatures to verify the genuineness of the curves.

A special Dewar vessel of Pyrex glass was made for studying the wing due to liquid oxygen. Two plane parallel Pyrex discs were fused parallel to each other in a horizontal position in the two walls at the bottom of the Dewar vessel. A Pyrex glass tube with blackened tail and closed at the lower end was placed inside the Dewar vessel with its tapered and blackened tail at the top. The Dewar vessel was then filled up with liquid oxygen filtered with filter paper. The liquid filled the inner tube by entering into it through a hole in its wall. The scattered light coming out through the bottom of the Dewar vessel was reflected by a right-angled prism and focussed with a long-focus lens on the entrance slit of the spectrophotometer. Finally, the record of the spectrum of the mercury lines reflected by gray paper was taken to compare the width of the peaks with those due to the scattered light.

RESULTS AND DISCUSSION

The records of the Raman spectra due to CCl_4 and $CHCl_3$ are reproduced in Figs. 3(a) and 3(b). The spectra of light scattered by benzene at 5°C and 75°C are reproduced in Figs. 4 and 5 respectively and Fig. 6 shows the spectrum due to liquid oxygen. The record of the spectrum of incident light is also reproduced in Fig. 7 for comparison.

It is evident from Fig. 4 that the wing due to benzene at 5°C shows two broad maxima at about 44 cm^{-1} and 73 cm^{-1} respectively with a continuous background between them and the curve due to benzene at 75°C given in Fig. 4 shows that there is only one inflexion at about 49 cm^{-1} and that the curve extends upto a shorter distance. Crystals of benzene at −10°C show three lines at 44, 60 and 100 cm^{-1} respectively (Sirkar and Ray, 1950) and the frequency-shifts increase to 48, 60 and 116 cm^{-1} respectively when the temperature of the crystals is lowered to −100°C. The broad maxima at 44 cm^{-1} and 73 cm^{-1} in the wing due to the benzene at 5°C may therefore correspond respectively to the lines 60 and 100 cm^{-1} due to the crystals at −10°C, the frequency-shifts diminishing with the rise of temperature from −10°C to 5°C and with the change of state. The band corresponding to the line 48 cm^{-1} of the crystal may have merged with the strong half-width of the Rayleigh line which extends up to about 38 cm^{-1} from the centre of the line in this case. All these facts show that these bands are not produced by the rotation of the molecules in the liquid state but they originate most probably from vibrations in groups of molecules which are formed in the liquid at 5°C and break up when the temperature is raised to 75°C. The

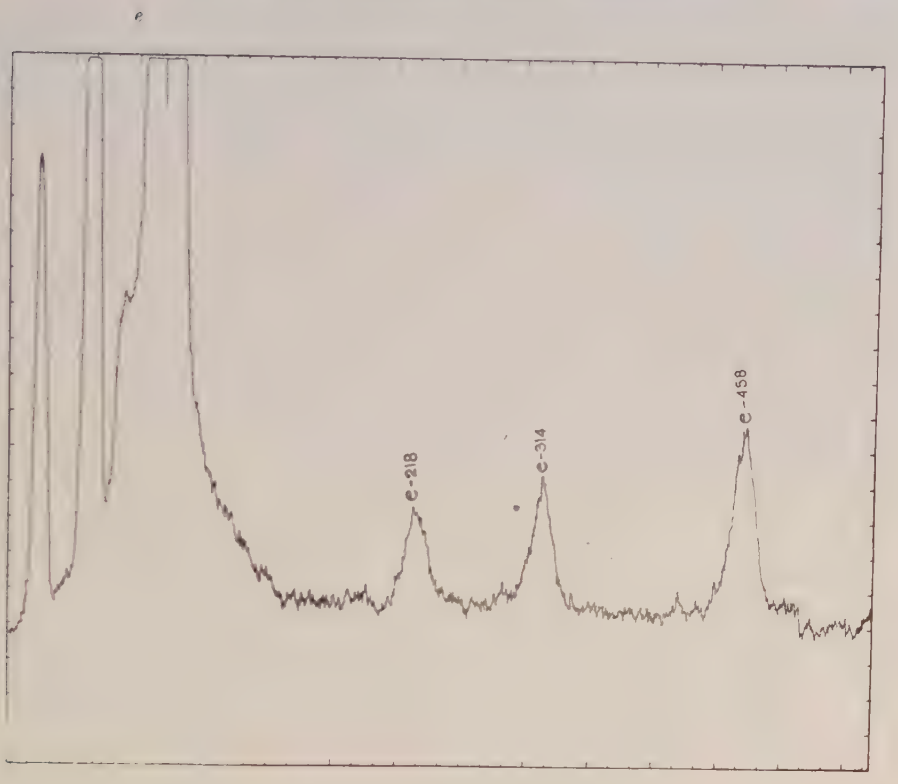

Fig. 3(a). Raman spectrum of CCl_4.

sharp lines observed in spectra of the crystals are therefore produced by such vibrations in groups of molecules, the intermolecular bond being slightly stronger in the case of the crystals. These results confirm the observations made by Kastha (1958) who studied the distribution of intensity in the wing of the Rayleigh line due to a few organic liquids at different temperatures and found evidence of formation of groups of molecules giving rise to continuous wing at temperatures a few degrees above the melting points of the substances.

A comparison of the curve due to the 4046 A line of Hg scattered by liquid oxygen reproduced in Fig. 6 with that due to the incident line shown in Fig. 7 indicates that the scattered line is much broader than the incident line probably due to the existence of a strong wing close to the Rayleigh line. The peak is unsymmetrical due to sulggishness if the pen during return sweep. It is further observed that on the Stokes sides of the 4046 A line the wing extends upto about 100 cm^{-1} from the centre of the Rayleigh line and there are inflexions at distances of about 38 cm^{-1}, 49 cm^{-1} and 60 cm^{-1}, the intensity falling off rapidly after each inflexion. It would be interesting to compare these results with those due to the gas. Unfortunately, the spectrum due to the gas at a temperature just above $-180°C$ has not been investigated by any

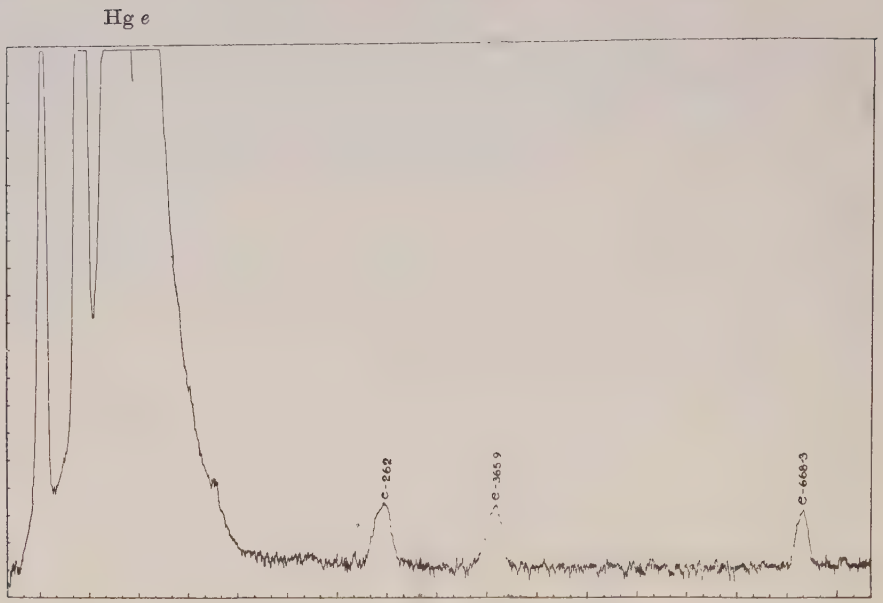

Fig. 3(b). Raman spectrum of $CHCl_3$.

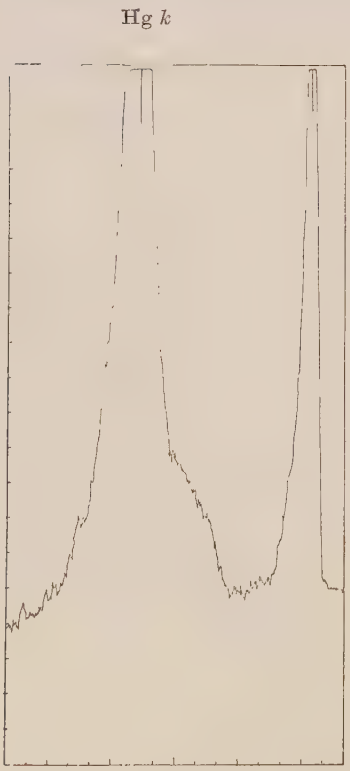

Fig. 4. 'Wing' due to benzene at 5°C.

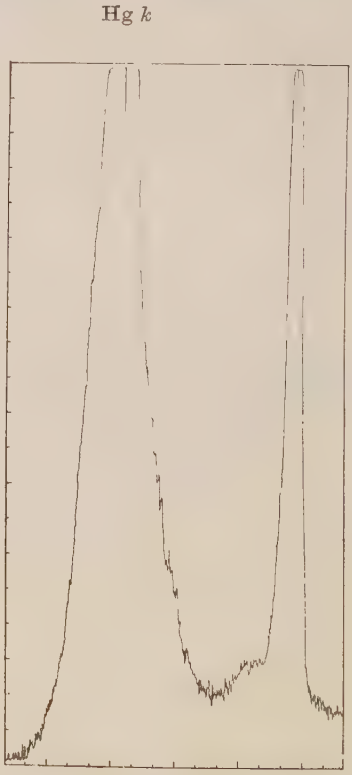

Fig. 5. 'Wing' due to benzene at 75°C.

previous worker. Theoretical values of the relative intensities of the rotational lines of O_2 at $-120°C$ are given in Table I.

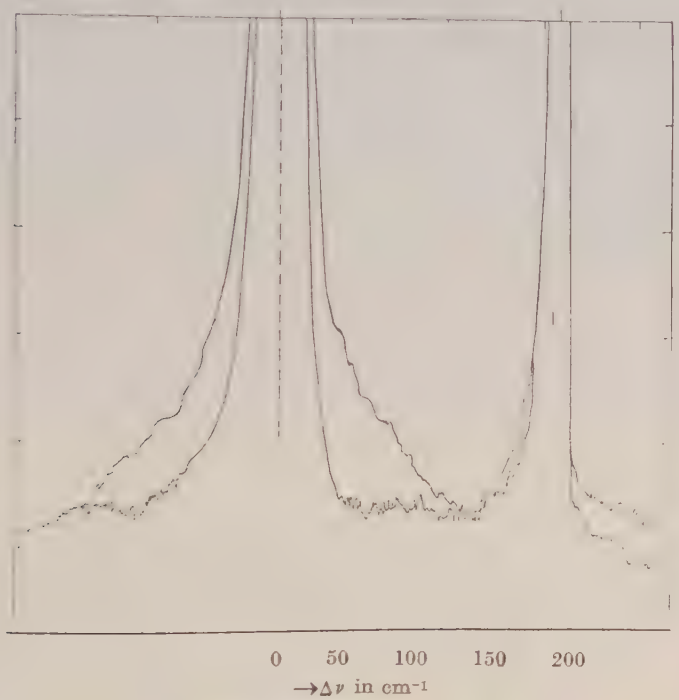

Fig. 6. Rotational wing due to liquid oxygen.

TABLE I

Initial value of J	$\Delta\nu$ in cm^{-1}	Relative intensity in arbitrary units
1	14.26	0.153
3	25.88	0.226
5	37.36	0.221
7	48.88	0.160
9	60.20	0.092
11	71.80	0.042

It can be seen from Table I that the second and third rotational Raman lines of O_2 are expected to be almost of the same intensity and the strongest lines in the rotational spectrum. The fourth line at about 49 cm^{-1} would be much weaker than either of these two lines and the fifth line should be less than half as intense as the second or the third line. The inflexions at 38 cm^{-1},

49 cm^{-1} and 60 cm^{-1} observed in the spectrum of liquid oxygen at −180°C agree closely with the rotational lines of O_2 at 180°C both in respect of positions and relative intensities. The appearance of broad inflexions in place of sharp peaks shows that the intermolecular collision in the liquid broadeus the lines.

The region from the edge of the Rayleigh line upto about 14 cm^{-1} would be free from any scattered intensity theoretically, but Fig. 6 shows an intense scattering in this region extending upto about 35 cm^{-1} and masking the two rotational maxima at about 14.26 cm^{-1} and 25.88 cm^{-1}. This broadening is not due to any difference in the intensities of the Rayleigh line and the inner incident line reproduced in Fig. 6, because the width of the line 4077 A is the same in both the cases. It has to be concluded, therefore, that probably some of the O_2 molecules form O_4 molecules with loose coupling between them so that the vibration and rotation of such dimeric molecules produce a strong wing extending upto about 35 cm^{-1} from the centre of the Rayleigh line.

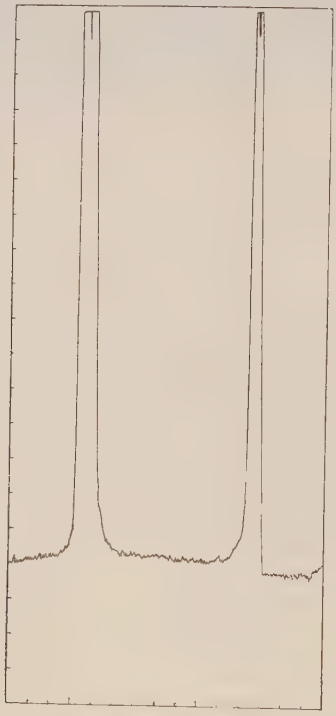

Fig, 7. Record of incident Hg lines.

The wing of the Rayleigh line due to liquid oxygen was studied previously by several workers by using prism spectrographs and photographic method. Saha (1940) first observed a continuous wing with a maximum at a distance of 50 cm^{-1} from the centre of the Rayleigh line. Later, Crawford *et al.* (1952) reported that they failed to detect any maximum in the continuous wing due to

liquid oxygen. Kastha repeated the investigation in 1954 and by carefully superposing the microphotometric record of the incident mercury line 4047 Å on that of the line scattered by liquid oxygen, found a maximum at 40 cm^{-1} from the Rayleigh line in the continuous wing due to liquid oxygen. The distances of the maximum found by Kastha (1954) is almost the same as that of the first inflexion observed in the present investigation, but the larger intensity upto 35 cm^{-1} from the edge of the Rayleigh line could not be detected by Kastha (1954) The photographic method is thus inferior to the photoelectric method for such an investigation when in the latter case a grating with high resolving power is used, so that the wing is clearly separated brom the Rayleigh line.

ACKNOWLEDGMENT

The authors' thanks are due to Dr. A. R. Deb who rendered some help in the intital stages of the construction of the spectrophotometer and to the staff of the workshop of the Association who made some parts of the spectrophotometer and assembled the different parts to make the complete instrument.

REFERENCES

Chien, Jen-Yuan and Bender, Paul, 1947, *J. Chem. Phys.*, **15**, 376.
Crawfold, M. F., Welsh, H. L. and Harrold, J. H., 1952, *Canad. J. Phys.*, **30**, 81.
Ebert, H., 1889, *Weid. Ann.*, **38**, 489.
Fastie, W. G., 1952, *J. Opt. Soc. America*, **52**, 641.
Kastha, G. S., 1954, *Ind. J. Phys.*, **28**, 329.
Kastha, G. S., 1958, *Ind. J. Phys.*, **32**, 473.
Saha, B., 1940, *Ind. J. Phys.*, **14**, 123.
Sirkar, S. C. and Ray, A. K., 1950, *Ind. J. Phys.*, **24**, 189.
Trumpy, B., 1933, *Z. f. Phys.*, **84**, 282.

43

STRUCTURE OF THE SPECTRUM OF DOUBLY IONISED BROMINE

Y. BHUPALA RAO

Oil and Natural Gas Commission, Dehra Dun

(*Received November* 17, 1960)

Plate VI and Plate VII (A and B)

ABSTRACT. The earlier analysis of the spectrum of Br III is revised and extended. A large number of levels belonging to the various configurations are newly identified, leading to the classification of more than 200 lines, which bring the total of classified lines to about 230. The doublets are correctly identified and are confirmed by the intercombinations with the quartets. The third ionisation potential of bromine given in the earlier analysis is verified to be correct.

INTRODUCTION

The first important investigation on the spectrum of doubly ionised bromine is by Bloch and Bloch (1927) who have given a fairly extensive list of the lines of Br III in the region 6600–2200A using a source of electodeless discharge. Lacroute (1935) has extended the list with measurements in the vacuum ultraviolet region on a 1-metre normal incidence vacuum grating spectrograph using a source of electrodeless discharge similar to the one employed by Bloch and Bloch.

Rao and Krishna Murty (1937) are the first to make a beginning towards the correct analysis of the structure of the spectrum. They have rejected the analysis given by Deb (1930) and successfully identified the deepest and fundamental quarters of the $4p^3$, 5s, 5p and 6s configurations and calculated the ionisation potential from the two members of the *ns* ^4P series. They have given a tentative list of some levels belonging to 4d and 5d configurations basing the assignments on the magnitude of the levels but without specific designation as that would be uncertain in the absence of other evidence.

They have also given a tentative identification of some of the doublets of $4p^3$, 5s and 5p configurations, independent of the quarters. The identifications are based, as stated by them, mainly on the detection of several pairs in the region below 1000A having the characteristic interval 1664 cm^{-1} which is of the order of the predicted interval $4p^3\ ^2P_{\frac{1}{2}}^0 - 4p^3\ ^2P_{1\frac{1}{2}}^0$. From these pairs the doublet groups $4p^3\ ^2D^0$, $^2P^0 - 5s\ ^2P$, $5s'\ ^2D$ are built up although some of the combinations are absent. By extrapolation into the shorter wavelength region some of the 5p doublet levels have been located. It is also remarked that some of the levels assigned to the 4d and 5d configurations might in fact be doublet levels. Pending

further investigation the publication of intercombinations was withheld. In a later communication Rao (1944) has reported the identification of a few intercombinations and has given the interval $4p^3\ {}^4S_{1\frac{1}{2}}{}^0 - 4p^3\ {}^2D_{1\frac{1}{2}}{}^0$ as 15042 cm^{-1}.

Moore (1952) has collected in the book "Atomic Energy Levels, Vol. II" all the energy levels given in the paper of Rao and Krishna Murty (1937) arranging them in the ascending order of magnitude with $4p^3\ {}^4S_{1\frac{1}{2}}$ as zero. She has added the correction 15042 cm^{-1} (Rao, 1944) to all the doublets starting with $4p^3\ {}^2D_{1\frac{1}{2}}{}^0$ as zero.

Still there remain quite a large number of lines unclassified, and the analysis is very far from complete and needs confirmation. In pursuance of the analysis obtained of the spectrum of Br II (Bhupala Rao, 1958), a revision of the analysis of the spectrum of Br III has been undertaken. The extensive experimental work on the spectrum done in connection with Br II has served for the purpose of this analysis also. The investigation has shown that while the quartet levels are confirmed, the doublets and intercombinations given by Rao and Krishna Murty (1937) and Rao (1944 and unpublished work) need revision except the level $4p^3\ {}^2D_{2\frac{1}{2}}{}^0$. A large number of new levels are also identified and intercombinations are definitely established leading to the classification of more than 200 additional lines bringing the total of classified lines to about 230.

EXPERIMENTAL

The sources of radiation and other details about excitation and recording of the spectrum are given in the paper on Br II (Bhupala Rao, 1958).

As already mentioned in the paper on Br II (Bhupala Rao, 1958) in addition to the data obtained from the experimental work at the Andhra University by the author, a large number of photographs were also kindly made available to the author by Prof. K. R. Rao and were of very great help. These pictures extending from 1085 to 480A were taken at Upsala with a Grazing Incidence Spectrograph long ago and well preserved. The dispersion was about 3.2A/mm near 950A. The sources consisted of a vacuum spark between electrodes tipped with Rb Br and Cs Br. Full details regarding the pictures are given by Rao and Badami (1931) in the paper on Se IV.

The lines of Br III are distinguished from the lines of Br II in the infra-red, visible and near ultraviolet regions by the criterion that a complete or partial suppression of the second and higher spark lines occurs when a suitable inductance is placed in the condensed discharge circuit while the intensity of the first spark lines either remains unaltered or increases. Several of the Br III lines are hazy and have large intense wings on the long wavelength side in the condensed discharge, which make their measurement difficult. The lines of Br. IV are comparatively sharp and are completely suppressed when the inductance is included in the circuit. Since some of the Br III lines also are completely suppressed on

including the inductance the behaviour of the lines in rectified discharge also is taken into consideration for distinguishing the lines of Br III from the lines of Br IV. In the rectified discharge, under suitable conditions, some of the Br IV lines appear with more intensity than in the condensed discharge. Though these criteria give fairly good results they are not entirely critical and cannot be depended upon to give absolutely correct results, because for a given ion lines from higher energy states behave in much the same way as those from next ion. In the vacuum ultraviolet region where lines from lower energy states occur, several lines of Br III appear in the inductance picture also with comparable intensity and it is difficult to distinguish them from the Br II lines. In this region a few higher stage spark lines also seem to be present in the inductance picture. An intensive examination of the entire spectrum and a line by line scrutiny has become necessary for the ultimate assignment.

All the lines of Br III classified in this investigation are given in Table II with their intensities in condensed discharge, wavelengths, wavenumbers and classifications. As in the case of Br II, in this paper also the wavelengths below 2000A are values in vacuum.

ANALYSIS

Br III is isoelectronic with As I, Se II, and Kr IV which have been respectively investigated by Meggers, Shenstone and Moore (1950), by Krishna Murty and Rao (1935) and Martin (1935) and by Boyce (1935) and Rao and Krishna Murty (1939). The structures of As I and Se II are almost completely known but the analysis of Kr IV is sketchy and far from complete.

The predicted terms of Br III are given in Table I. Terms identified completely or partially are underlined. Those identified in the earlier investigations are marked with an asterisk also. All the newly identified levels are already given in the preliminary note (Bhupala Rao, 1956) in the ascending order of magnitude based on $4p^3\ {}^4S^0_{1\frac{1}{2}}$ as zero. Following the notation adopted by Moore (1952) levels arising from the ^1D and ^1S states of the Br IV ion are distinguished by affixing a single prime and a double prime respectively to the running electron.

The analysis presented in this paper shows that there is a considerable overlapping of the terms of the same configuration and also of the terms of different configurations. The term intervals are as large as and sometimes even larger than the separations between the neighbouring terms showing very great departure from L-S coupling. The ratios of the intervals of the individual terms also show large deviations from the values predicted on the basis of L-S coupling. Unlike in Br II the combinations between even and odd levels are not profuse and it makes the analysis very difficult. Particularly, the combinations between the doublets of even and odd configurations are only a few. Some of the doublets give more combinations with the quartets than with the doublets, the intercombinations being thus relatively more intense.

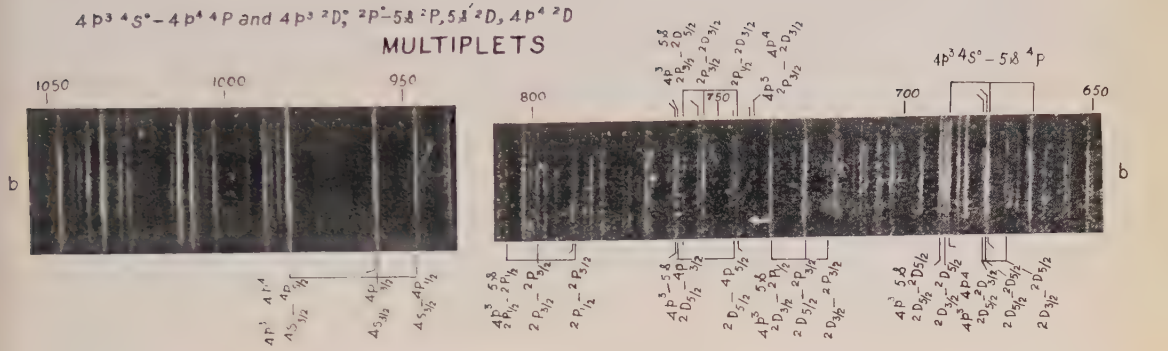
4p³ ⁴S°–4p⁴ ⁴P and 4p³ ²D°, ²P°–5s ²P, 5s ²D, 4p⁴ ²D
MULTIPLETS
4p³ 4S°–5s ⁴P
1050
1000
950
800
750
700
650
b
b

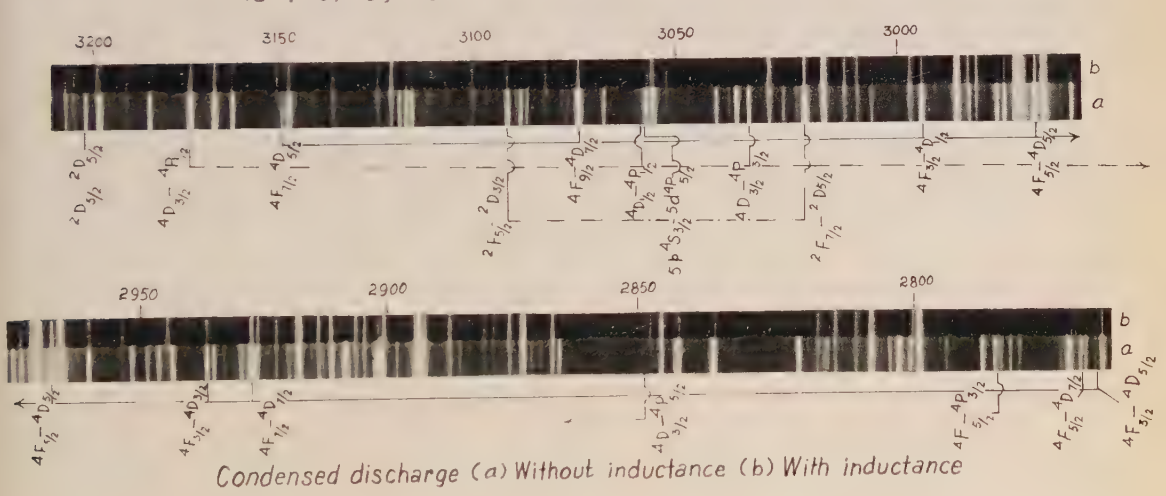
4d ⁴F –5p ⁴D°, 4d ⁴D –5p ⁴P° and 4d ²F – 5p ²D° MULTIPLETS
3200
3150
3100
3050
3000
2950
2900
2850
2800
b
a
b
a
Condensed discharge (a) Without inductance (b) With inductance

Indian Journal of Physics, Vol. XXXV, No. 8

PLATE VII A

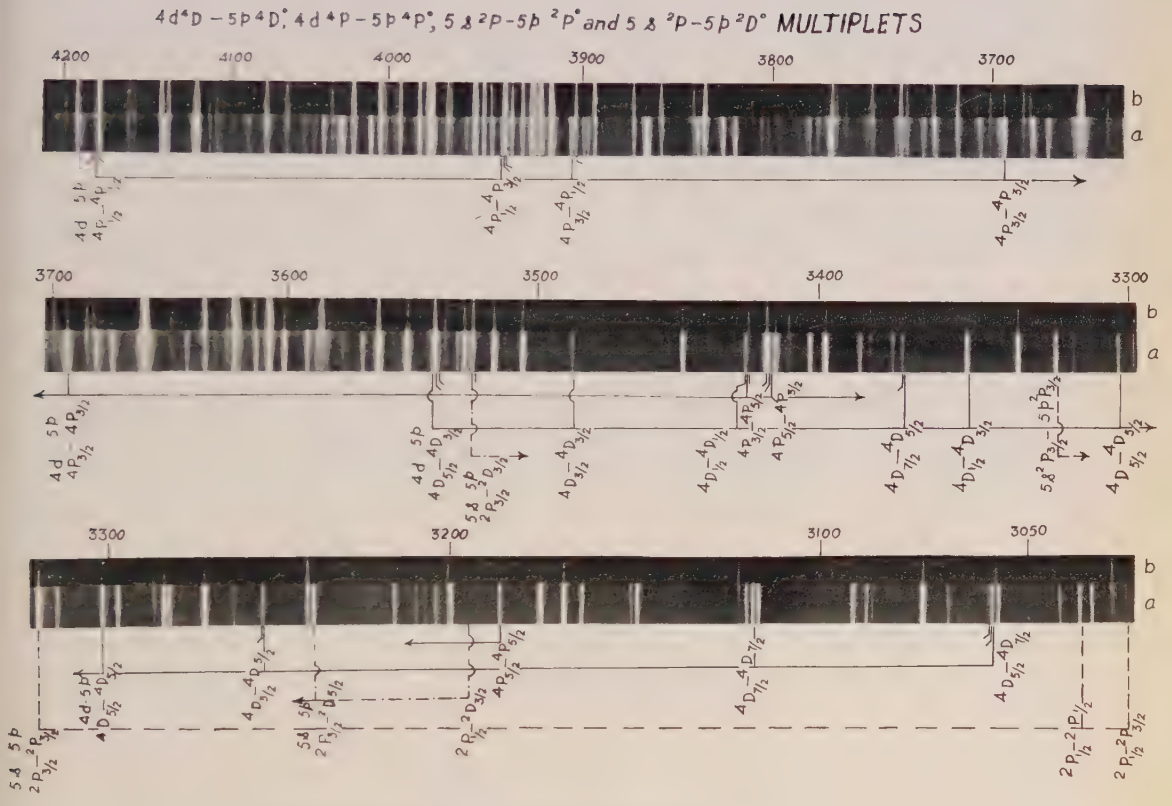

Condensed discharge (a) Without inductance (b) With inductance

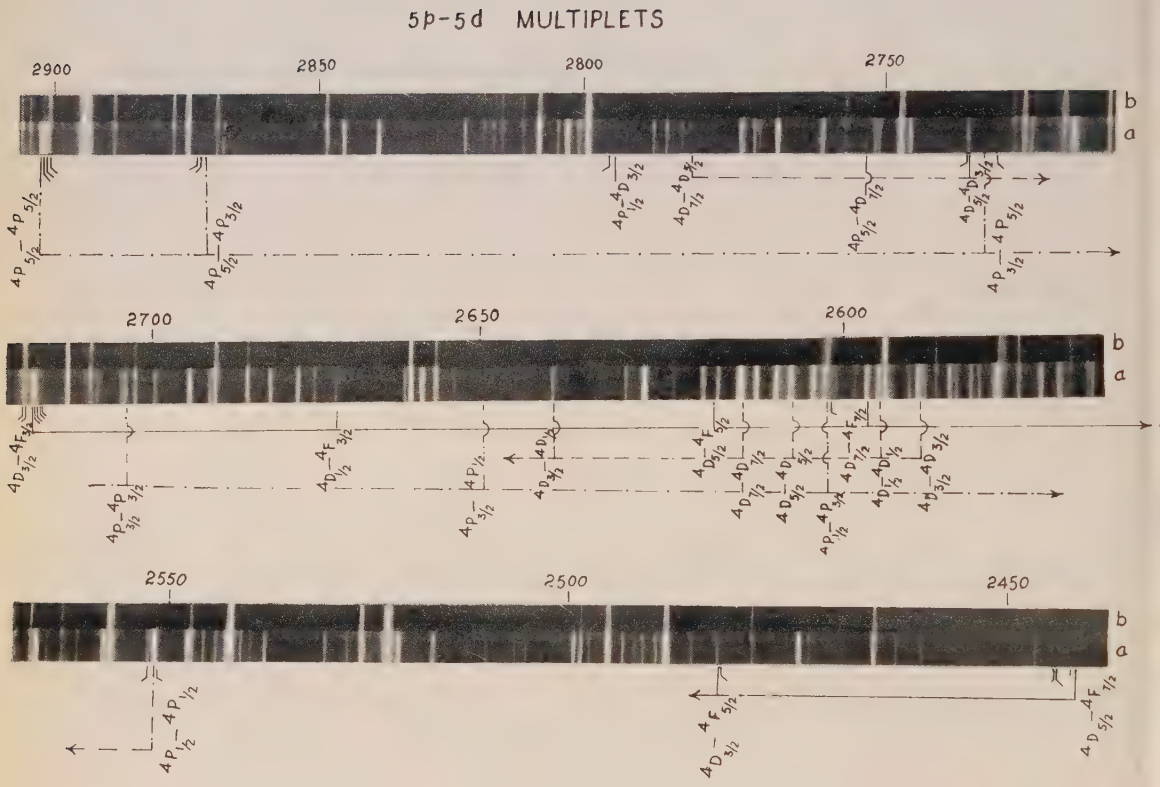

Condensed discharge (a) Without inductance (b) With inductance

A careful examination of the plates has confirmed the previous identification of the quartets of $4p^3$, 5s, 5p and 6s configurations. The intensity and behaviour of the lines are in conformity with the classifications. Examination of the doublets previously suggested is then taken up. A series of trials have been made to enlarge the scheme of classification assuming Rao and Krishna Murthy's identification of doublets as correct. All the attempts have proved to be unsuccessful. It is presumed that it is the failure to make correct assignment of the doublets and the intercombinations with the quartets that might have led to difficulty in extending the analysis further by Rao and Krishna Murty themselves. Therefore an independent and fresh approach to the identification of doublets is made with the aid of the irregular doublet law. The application of the irregular doublet law in the manner done by Bowen and Millikan and used by Rao (1927) in the analysis of the Sn III spectrum for transitions where the principal quantum number changes, is employed. By comparing with the values in As I and Se II using the irregular doublet law, the positions for the $4p^3\ {}^2D_{2\frac{1}{2}}{}^0-5s\ {}^2P_{1\frac{1}{2}}$, $4p^3\ {}^2D_{1\frac{1}{2}}{}^0-5s\ {}^2P_{\frac{1}{2}}$, $4p^3\ {}^2P_{1\frac{1}{2}}{}^0-5s\ {}^2P_{1\frac{1}{2}}$ and $4p^3\ {}^2P_{\frac{1}{2}}{}^0-5s\ {}^2P_{\frac{1}{2}}$ combinations in Br III are calculated to be 136387, 133843, 123902 and 121705 cm^{-1} respectively. With the help of these calculated values and the predicted intervals for the $4p^3\ {}^2D^0$, ${}^2P^0$ and 5s ${}^2p$ terms the identifications of the doublets are made. With the assignments of Rao and Krishna Murty no intercombinations between the 5s ${}^2P$ levels and the 5p quarters could be observed. With the present choice the intercombination lines are observed in the calculated positions. Also, the intensities of the lines confirm the present assignments. From these it has been possible to establish the $4p^3\ {}^2D^0$, ${}^2P^0$, $4p^4\ {}^2D$, 5s ${}^2P$ and 5s′ ${}^2D$ terms. The identification of the 5s′ ${}^2D$ and $4p^4\ {}^2D$ terms proved to be more difficult because of the intensity anomalies in their combinations and their proximity to each other. Starting with the doublets of the 5s configuration and by a comparison of the position of $np^2(n-1)s\ {}^2P_{1\frac{1}{2}}-np^2(n-1)p\ {}^2P_{1\frac{1}{2}}{}^0$ combinations in the spectra isoelectonic with F III, Cl III and Br III the $5p\ {}^2P_{1\frac{1}{2}}{}^0$, ${}^2D_{2\frac{1}{2}}{}^0$ levels are located at 105581.0 and 107331.0 respectively. Proceeding from these with the help of the estimated intervals of the 5p doublets the 5p ${}^2D^0$, ${}^2P^0$ and ${}^2S^0$ terms are identified completely. This also proved somewhat difficult because of the poor development of the multiplets. The 5p doublets combine only with a few of the terms of the even configurations. Attempts to identify the 5p′ doublet levels with the help of the 5s′ ${}^2D$ interval have been unsuccessful. The transitions between the doublets of $4p^3$ and 5s, $4p^4$ configurations are shown in Plate VI and the combinations between the doublets of 5s and 5p configurations in Plate VIIA.

From a study of the position of the $4p^3\ {}^4S^0-4p^4\ {}^4P$ multiplet and the intervals of the $4p^4\ {}^4P$ term in spectra isoelectonic with F III, Cl III and Br III this multiplet in Br III is estimated to be in the region 100,000 – 110,000 cm^{-1} with ${}^4P_{\frac{1}{2}}-{}^4P_{1\frac{1}{2}}$ and ${}^4P_{1\frac{1}{2}}-{}^4P_{2\frac{1}{2}}$ intervals of the order of −1260 and −2650 respectively. After a close scrutiny of the plates for three lines in that region with the estimated

intervals, the lines 105380, 104129 and 101532 cm^{-1} are classified as the combinations respectively of $4p^4\ {}^4P_{\frac{1}{2},1\frac{1}{2},2\frac{1}{2}}$ levels with $4p^3\ {}^4S_{1\frac{1}{2}}{}^0$. Their intervals -1251 and -2597 agree well with the predicted values. These classifications are confirmed by the large number of combinations between the resulting levels and the 5p quartet terms. The $4p^3\ {}^4S^0-4p^4\ {}^4P$ multiplet is shown in Plate VI.

Rao and Krishna Murty (1937) have assigned nine levels to the 4d configuration on consideration of their magnitude. But they have stated that some of them might actually be doublet levels. Attempts to identify the 4d levels starting with the 5p $^4D^0$ and $^4P^0$ intervals have resulted in the identification of the $4p^4\ {}^2P$ term, all the 4d quartets, the 4d ^2F term, the 4d $^2D_{1\frac{1}{2}}$, $^2P_{1\frac{1}{2}}$ levels and three other levels designated 1, 2 and 3. Of the nine given by Rao and Krishna Murty, only the five levels 2, 3, 5, 6 and 9 are found to be real, and of these the level 2 is identified as $4p^4\ {}^2P_{1\frac{1}{2}}$. The $4p^4\ {}^2P$ term does not combine with any of the $4p^3$ levels.

The 4d ^4F, ^4D terms combine well with the 5p $^4D^0$ term, but seldom with 5p $^4P^0$ term. In the case of the 4d ^4P term, the 4d $^4P-5p\ {}^4P^0$ multiplet and 4d $^4P_{1\frac{1}{2}}-5p\ {}^4D_{\frac{1}{2}}{}^0$, 4d $^4P_{\frac{1}{2}}-5p\ {}^4S^0{}_{1\frac{1}{2}}$ and 4d $^4P_{1\frac{1}{2}}-5p\ {}^2P_{1\frac{1}{2}}{}^0$ combinations alone could be located. Except for two lines the 4d levels do not give any combinations with the 5p $^2P^0$ and $^2S^0$ terms. Even with the 5p $^2D^0$ term the combinations are only a few. The 4d ^4P term is inverted while the other terms are regular. But none of these is in conformity with L—S coupling. The 4d $^4F-5p\ {}^4D^0$, 4d $^4D-5p\ {}^4D^0$ and 4d $^4P-5p\ {}^4P^0$ multiplets are shown in Plates VI and VIIA.

The 5d quartet terms also are arrived at with the help of the intervals of the 5p quartets. Only two, 11 and 13, of the seven levels 10 to 16 assigned by Rao and Krishna Murty to the 5d configuration, could be confirmed. The 5d terms exhibit combining characteristics similar to the 4d terms and their combinations with the odd levels are not profuse. Here too the term intervals are not regular and show large deviations from L-S coupling. The 5d ^4P term also is inverted. This inversion of the nd ^4P term is a feature present in the spectra of F III and Cl III also.

The diagonal lines of the 5p $^4D^0-5d\ {}^4F$ multiplet are diminishing in intensity with increasing J values. From this trend in the variation of intensity the combination 5p $^4D_{3\frac{1}{2}}{}^0-5d\ {}^4F_{4\frac{1}{2}}$ is expected to be very weak, and since this is the only combination the 5d $^4F_{4\frac{1}{2}}$ level gives with the 5p levels, it is not found possible to fix this line. Consequently the 5d $^4F_{4\frac{1}{2}}$ level is not identified. The 5p $^4D^0-5d\ {}^4F$, 5p $^4D^0-5d\ {}^4D$ and 5p $^4P^0-5d\ {}^4P$ multiplets are marked on Plate VIIB.

The doublets of the 5d and 6s configurations are all expected to be of the same order of magnitude and it is not possible to distinguish between the levels of the two configurations. So, all these levels are designated arbitrarily by numerals 4 to 22.

TABLE I

Terms of Br III

Configuration	Terms				
$4s^2\ 4p^3$	$^4S^{0*}$	$^2D^0$	$^2P^0$		
$4s\ 4p^4$	^4P	^2P	^2D	^2S	
Basic terms of Br IV $4s^2\ 4p^2$	^3P		^1D	^1S	
$4s^2\ 4p^2\ 5s$	$^4P^*$ ^2P		^2D	^2S	
$4s^2\ 4p^2\ 4d$	^4F ^4D ^4P	^2G ^2F ^2D	^2F ^2S	^2D	
	^2F ^2D ^2P				
$4s^2\ 4p^2\ 5p$	$^4D^{0*}$ $^4P^{0*}$ $^4S^{0*}$	$^2F^0$ $^2D^0$	$^2P^0$	$^2P^0$	
	$^2D^0$ $^2P^0$ $^2S^0$				
$4s^2\ 4p^2\ 6s$	$^4P^*$ ^2P		^2D	^2S	
$4s^2\ 4p^2\ 5d$	^4F ^4D ^4P	^2G ^2F ^2D	^2P ^4S	^2D	
	^2F ^2D ^2P				
$4s^2\ 4p^2\ 6p$	$^4D^0$ $^4P^0$ $^4S^0$ $^2D^0$ $^2P^0$ $^2S^0$	$^2F^0$ $^2D^0$	$^2P^0$	$^2P^0$	

*.....Identified in previous investigations.

TABLE II

Newly classified lines of Br III

Intensity	λ(air)	ν(vac)	Classification	Remarks
0bh	7696.1	12990	$5d\ ^4F_{3\frac{1}{2}}-23^0$	
2	7673.1	13029	$4p^4\ ^2D_{1\frac{1}{2}}-5p\ ^4P^0_{\frac{1}{2}}$	
2	7192.8	13899	$6s\ ^4P_{2\frac{1}{2}}-23^0$	
00b	6899.8	14489	$4p^4\ ^2D_{1\frac{1}{2}}-5p\ ^4P^0_{1\frac{1}{2}}$	Br II line
1	6459.21	15477.5	$5s'\ ^2D_{1\frac{1}{2}}-5p\ ^4P^0_{\frac{1}{2}}$	
1hb	5947.90	16808.0	$6s\ ^4P_{1\frac{1}{2}}-23^0$	
1	5764.09	17344.0	$5d\ ^4P_{1\frac{1}{2}}-24^0$	
1	5693.40	17559.3	$11-24^0$	
2	5446.80	18354.3	$4p^4\ ^2D_{2\frac{1}{2}}-5p\ ^2D^0_{1\frac{1}{2}}$	
0	5440.38	18376.0	$4p^4\ ^2D_{1\frac{1}{2}}-5p\ ^4S^0_{1\frac{1}{2}}$	Br II line

TABLE II (*contd.*)

Intensity	λ(air)	ν(vac)	Classification		Remarks
00	5245.25	19059.6	5s′	$^2D_{1\frac{1}{2}}-5p$ $^4P^0_{2\frac{1}{2}}$	
3	5175.87	19315.1	4d	$^2P_{1\frac{1}{2}}-5p$ $^4D^0_{\frac{1}{2}}$	
1	5146.32	19426.0	6s	$^4P_{1\frac{1}{2}}-24^0$	
0	4896.67	20416.4	5p	$^2P^0_{\frac{1}{2}}-6$	
1	4803.14	20813.9	5s′	$^2D_{1\frac{1}{2}}-5p$ $^2S^0_{\frac{1}{2}}$	
00	4661.58	21446.0	5p	$^4S^0_{1\frac{1}{2}}-5$	
3	4556.49	21940.6	5s′	$^2D_{2\frac{1}{2}}-5p$ $^2D^0_{1\frac{1}{2}}$	
4	4519.74	22119.0	4d	$^4P_{1\frac{1}{2}}-5p$ $^4D^0_{\frac{1}{2}}$	
3	4393.51	22754.5	5s′	$^2D_{1\frac{1}{2}}-5p$ $^2P^0_{1\frac{1}{2}}$	
3	4383.91	22804.3	4d	$^2P_{1\frac{1}{2}}-5p$ $^4P^0_{\frac{1}{2}}$	
1	4319.49	23144.4	5p	$^4S^0_{1\frac{1}{2}}-7$	
0	4316.15	23162.3	4d	$^2D_{1\frac{1}{2}}-5p$ $^4P^0_{\frac{1}{2}}$	
1hb	4219.15	23694.8		$3-5p$ $^4P^0_{\frac{1}{2}}$	
1h	4190.82	23855.0		$2-5p$ $^4D^0_{\frac{1}{2}}$	
1	4181.73	23906.8	4d	$^4P_{\frac{1}{2}}-5p$ $^4P^0_{\frac{1}{2}}$	
00vb	4166.58	23993.8	5p	$^4P^0_{2\frac{1}{2}}-6$	
3	4120.34	24263.0	4d	$^2P_{1\frac{1}{2}}-5p$ $^4P^0_{1\frac{1}{2}}$	
2H	4116.70	24284.5	5s	$^2P_{1\frac{1}{2}}-5p$ $^4P^0_{1\frac{1}{2}}$	
			4d	$^2F_{3\frac{1}{2}}-5p$ $^4D^0_{2\frac{1}{2}}$	
3hb	4086.63	24463.2	5s′	$^2D_{2\frac{1}{2}}-5p$ $^2D^0_{2\frac{1}{2}}$	Br II line
00b	4078.36	24512.8		$2-5p$ $^4D^0_{1\frac{1}{2}}$	
0Hb	4059.99	24623.7	4d	$^2D_{1\frac{1}{2}}-5p$ $^4P^0_{1\frac{1}{2}}$	
0	3977.83	25131.3	5p	$^4P^0_{1\frac{1}{2}}-4$	
0b	3974.34	25154.3		$3-5p$ $^4P^0_{1\frac{1}{2}}$	
0	3963.18	25225.2	5p	$^4S^0_{1\frac{1}{2}}-8$	
0	3946.00	25335.0	5p	$^4P^0_{1\frac{1}{2}}-5$	
00	3941.13	25366.3	4d	$^4P_{\frac{1}{2}}-5p$ $^4P^0_{1\frac{1}{2}}$	
4	3903.95	25607.9	4d	$^4P_{1\frac{1}{2}}-5p$ $^4P^0_{\frac{1}{2}}$	
0b	3880.25	25764.3	5s	$^2P_{\frac{1}{2}}-5p$ $^4P^0_{\frac{1}{2}}$	
2hb	3838.34	26045.6	4d	$^2F_{2\frac{1}{2}}-5p$ $^4D^0_{2\frac{1}{2}}$	
2	3788.67	26387.0	4d	$^2P_{1\frac{1}{2}}-5p$ $^4P^0_{2\frac{1}{2}}$	

TABLE II (*contd.*)

Intensity	λ(air)	ν(vac)	Classification	Remarks
2	3785.77	26407.2 5s	$^2P_{1\frac{1}{2}}-5p\ ^4P^0_{2\frac{1}{2}}$	
0h	3760.72	26583.1	$2\ -5p\ ^4D^0_{2\frac{1}{2}}$	
00	3744.57	26697.1 4d	$^2F_{3\frac{1}{2}}-5p\ ^4D^0_{3\frac{1}{2}}$	Br II line
1	3731.07	26794.4 5p	$^4P^0_{\frac{1}{2}}-5$	
2h	3724.75	26839.8 5p	$^4D^0_{3\frac{1}{2}}-7$	
2b	3704.01	26990.1 5p	$^4P^0_{2\frac{1}{2}}-8$	
5	3693.53	27066.7 4d	$^4P_{1\frac{1}{2}}-5p\ ^4P^0_{1\frac{1}{2}}$	
00	3672.22	27223.8 5s	$^2P_{\frac{1}{2}}\ -5p\ ^4P^0_{1\frac{1}{2}}$	Br II line
0	3655.12	27351.1 5p	$^4D^0_{2\frac{1}{2}}-4$	
3	3612.33	27675.1	$1-5p\ ^4D^0_{1\frac{1}{2}}$	
6	3551.08	28152.4 4d	$^2P_{1\frac{1}{2}}-5p\ ^4S^0_{1\frac{1}{2}}$	
00	3543.29	28214.3 4d	$^4D_{2\frac{1}{2}}-5p\ ^4D^0_{1\frac{1}{2}}$	
2	3531.54	28308.2 5p	$^4P^0_{2\frac{1}{2}}-9$	
4	3528.86	28329.7 4d	$^2P_{1\frac{1}{2}}-5p\ ^2D^0_{1\frac{1}{2}}$	?
2	3527.98	28336.8 5p	$^4D^0_{2\frac{1}{2}}-6$	Br II line
3	3526.07	28352.1 5s	$^2P_{1\frac{1}{2}}-5p\ ^2D^0_{3\frac{1}{2}}$	
0	3512.97	28457.8 4d	$^2F_{2\frac{1}{2}}-5p\ ^4D^0_{\frac{1}{2}}$	
6	3506.47	28510.6 4d	$^2D_{1\frac{1}{2}}-5p\ ^4S^0_{1\frac{1}{2}}$	
2	3487.63	28664.6 4d	$^4D_{1\frac{1}{2}}-5p\ ^4D^0_{1\frac{1}{2}}$	
2	3433.96	29112.6 5p	$^4P^0_{1\frac{1}{2}}-8$	
3vb	3425.29	29186.3 4d	$^4D_{\frac{1}{2}}-5p\ ^4D^0_{\frac{1}{2}}$	
1	3424.89	29189.7 4d	$^4P_{1\frac{1}{2}}-5p\ ^4P^0_{2\frac{1}{2}}$	
5	3417.61	29251.9 5p	$^4D^0_{2\frac{1}{2}}-7$	
2h	3417.23	29255.1 4d	$^4P_{\frac{1}{2}}-5p\ ^4S^0_{1\frac{1}{2}}$	Br II line
2b	3416.39	29262.3 4d	$^4P_{2\frac{1}{2}}-5p\ ^4P^0_{1\frac{1}{2}}$	
3	3397.88	29421.7 5p	$^4D^0_{1\frac{1}{2}}-4$	Br II line
2	3370.94	29656.8 4d	$^4D_{3\frac{1}{2}}-5p\ ^4D^0_{2\frac{1}{2}}$	
5	3349.75	29844.4 4d	$^4D_{\frac{1}{2}}-5p\ ^4D^0_{1\frac{1}{2}}$	
6	3321.08	30102.1 5s	$^2P_{1\frac{1}{2}}-5p\ ^2P^0_{1\frac{1}{2}}$	
5	3301.21	30283.2 4d	$^4D_{2\frac{1}{2}}-5p\ ^2D^0_{2\frac{1}{2}}$	
00b	3287.71	30407.6 5p	$^4D^0_{1\frac{1}{2}}-6$	

TABLE II (*contd.*)

Intensity	λ(air)	ν(vac)	Classification	Remarks
2b	3285.21	30430.7	5p $^4P^0_{1\frac{1}{2}}$—9	
1b	3277.15	30505.6	1—5p $^4P^0_{\frac{1}{2}}$	
5	3270.07	30571.6	5p $^4P^0_{\frac{1}{2}}$—8	
3	3252.74	30734.5	4d $^4D_{1\frac{1}{2}}$—5p $^4D^0_{2\frac{1}{2}}$	
5	3237.98	30874.6	5s $^2P_{1\frac{1}{2}}$—5p $^2D^0_{2\frac{1}{2}}$	
4	3214.59	31099.2	5s $^2P_{\frac{1}{2}}$ —5p $^2S^0_{\frac{1}{2}}$	
4	3202.90	31212.7	4d $^2D_{1\frac{1}{2}}$—5p $^2D^0_{2\frac{1}{2}}$	
0	3194.85	31291.4	5s $^2P_{\frac{1}{2}}$ —5p $^2D^0_{1\frac{1}{2}}$	
4	3185.21	31386.1	4d $^4P_{2\frac{1}{2}}$—5p $^4P^0_{2\frac{1}{2}}$	
5	3174.15	31495.4	4d $^4D_{1\frac{1}{2}}$—5p $^4P^0_{\frac{1}{2}}$	
4	3149.36	31743.3	4d $^4F_{3\frac{1}{2}}$—5p $^4D^0_{2\frac{1}{2}}$	
0bh	3134.75	31891.3	5p $^4P^0_{\frac{1}{2}}$—9	
0bh	3133.04	31908.7	5p $^2P_{1\frac{1}{2}}$—5d $^4P_{\frac{1}{2}}$	
00h	3127.41	31966.1	1—5p $^4P^0_{1\frac{1}{2}}$	
7	3117.29	32069.9	4d $^4D_{3\frac{1}{2}}$—5p $^4D^0_{3\frac{1}{2}}$	
7	3091.94	32332.8	4d $^2F_{2\frac{1}{2}}$—5p $^2D^0_{1\frac{1}{2}}$	
10	3074.42	32517.0	4d $^4F_{4\frac{1}{2}}$—5p $^4D^0_{3\frac{1}{2}}$	
1H	3059.60	32674.5	4d $^4D_{\frac{1}{2}}$ —5p $^4P^0_{\frac{1}{2}}$	Br II line
2hb	3058.49	32686.4	5p $^4S^0_{1\frac{1}{2}}$—5d $^4P_{2\frac{1}{2}}$	
5	3057.57	32696.2	4d $^4D_{2\frac{1}{2}}$—5p $^4D^0_{3\frac{1}{2}}$	
2h	3042.08	32862.7	5p $^4S^0_{1\frac{1}{2}}$—11	?
00	3040.04	32884.8	4d $^4P_{1\frac{1}{2}}$—5p $^2P^0_{1\frac{1}{2}}$	
7	3036.45	32923.6	5s $^2P_{\frac{1}{2}}$ —5p $^2P^0_{\frac{1}{2}}$	
6	3033.63	32954.2	4d $^4D_{1\frac{1}{2}}$—5p $^4P^0_{1\frac{1}{2}}$	
4	3025.63	33041.4	5s $^2P_{\frac{1}{2}}$ —5p $^2P^0_{1\frac{1}{2}}$	
0	3022.17	33079.2	5p $^4S^0_{1\frac{1}{2}}$—5d $^4P_{1\frac{1}{2}}$	
10	3020.76	33094.6	4d $^2F_{3\frac{1}{2}}$—5p $^2D^0_{2\frac{1}{2}}$	
8	2994.04	33390.0	4d $^4F_{1\frac{1}{2}}$—5p $^4D^0_{\frac{1}{2}}$	
7	2969.00	33671.6	4d $^4F_{2\frac{1}{2}}$—5p $^4D^0_{2\frac{1}{2}}$	
0hb	2952.88	33855.4	5p $^4P^0_{2\frac{1}{2}}$—5d $^4F_{2\frac{1}{2}}$	

TABLE II (*contd.*)

Intensity	λ(air)	ν(vac)	Classification	Remarks
3vbh	2946.26	33931.4	5p $^4P^0_{\frac{1}{2}}$ – 5d $^4F_{\frac{1}{2}}$	
6	2936.22	34047.5	4d $^4F_{\frac{1}{2}}$ – 5p $^4D^0_{1\frac{1}{2}}$	
2	2932.68	34088.6	1 – 5p $^4P^0_{2\frac{1}{2}}$	
8	2926.96	34155.2	4d $^4F_{3\frac{1}{2}}$ – 5p $^4D^0_{3\frac{1}{2}}$	
4	2901.89	34450.2	5p $^4P^0_{2\frac{1}{2}}$ – 5d $^4P_{2\frac{1}{2}}$	
4	2901.00	34460.8	5s $^4P_{2\frac{1}{2}}$ – 5p $^2D^0_{2\frac{1}{2}}$	
1h	2869.11	34843.8	5p $^4P^0_{2\frac{1}{2}}$ – 5d $^4P_{1\frac{1}{2}}$	
00b	2852.83	35042.6	5p $^4P^0_{3\frac{1}{2}}$ – 5d $^4D_{\frac{1}{2}}$	
2h	2849.91	35078.5	4d $^4D_{1\frac{1}{2}}$ – 5p $^4P^0_{2\frac{1}{2}}$	
2h	2843.79	35154.0	5p $^4S^0_{1\frac{1}{2}}$ – 13	
0h	2837.56	35231.2	4p^4 $^2P_{\frac{1}{2}}$ – 5p $^4D^0_{1\frac{1}{2}}$	
6	2804.16	35650.8	4p^4 $^2P_{1\frac{1}{2}}$ – 5p $^4D^0_{\frac{1}{2}}$	
3	2793.97	35780.8	5p $^4P^0_{\frac{1}{2}}$ – 5d $^4D_{1\frac{1}{2}}$	
6b	2785.28	35892.5	4d $^4F_{2\frac{1}{2}}$ – 5p $^4P^0_{1\frac{1}{2}}$	
3b	2784.21	35906.3	5p $^4S^0_{1\frac{1}{2}}$ – 14	
3	2781.09	35946.5	5p $^4D^0_{3\frac{1}{2}}$ – 5d $^4D_{2\frac{1}{2}}$	
8H	2772.62	36056.4	5p $^4P^0_{\frac{1}{2}}$ – 10	
6	2770.50	36083.9	4d $^4F_{2\frac{1}{2}}$ – 5p $^4D^0_{3\frac{1}{2}}$	
2	2767.89	36118.0	4d $^4F_{1\frac{1}{2}}$ – 5p $^4D^0_{2\frac{1}{2}}$	
?	2766.26	36139.2	5p $^4P^0_{1\frac{1}{2}}$ – 5d $^4D_{2\frac{1}{2}}$	
0h	2765.93	36143.6	5p $^4P^0_{2\frac{1}{2}}$ – 12	
3	2753.35	36308.7	4p^4 $^2P_{1\frac{1}{2}}$ – 5p $^4D^0_{1\frac{1}{2}}$	
4H	2752.06	36325.7	5p $^4P^0_{2\frac{1}{2}}$ – 5d $^4D_{3\frac{1}{2}}$	
3H	2747.18	36390.2	4d $^4D_{2\frac{1}{2}}$ – 5p $^4S^0_{1\frac{1}{2}}$	
2H	2742.36	36454.2	5p $^2P^0_{\frac{1}{2}}$ – 17	?
7H	2735.83	36541.2	5p $^4D^0_{2\frac{1}{2}}$ – 5d $^4D_{1\frac{1}{2}}$	
00	2733.43	36573.3	5p $^4P^0_{1\frac{1}{2}}$ – 5d $^4P_{2\frac{1}{2}}$	
			4d $^4D_{2\frac{1}{2}}$ – 5p $^2D^0_{1\frac{1}{2}}$	?
1h	2731.35	36601.1	5s $^4P_{\frac{1}{2}}$ – 5p $^4S^0_{1\frac{1}{2}}$	
1	2720.15	36751.8	5p $^4P^0_{1\frac{1}{2}}$ – 11	

TABLE II (*contd.*)

Intensity	λ(air)	ν(vac)	Classification	Remarks
3h	2719.39	36762.1	5p $^4D^0_{1\frac{1}{2}}$ — 5d $^4F_{1\frac{1}{2}}$	
00	2715.37	36816.5	5p $^4D^0_{2\frac{1}{2}}$ — 10	
1	2710.83	36878.2	4d $^4F_{1\frac{1}{2}}$ — 5p $^4P^0_{\frac{1}{2}}$	
4	2704.28	36967.5	5p $^4P^0_{1\frac{1}{2}}$ — 5d $^4P_{1\frac{1}{2}}$	
7h	2671.53	37420.6	5p $^4D^0_{\frac{1}{2}}$ — 5d $^4F_{1\frac{1}{2}}$	
2	2649.82	37727.2	5p $P^0_{1\frac{1}{2}}$ — 5d $^4P_{\frac{1}{2}}$	
0	2645.19	37793.2	5p $^4P^0_{1\frac{1}{2}}$ — 6s $^4P_{2\frac{1}{2}}$	
7h	2639.60	37873.3	5p $^4D^0_{1\frac{1}{2}}$ — 5d $^4D_{\frac{1}{2}}$	
4	2632.88	37969.9	5p $^2D^0_{2\frac{1}{2}}$ — 21	
7h	2629.23	38022.6	4d $^4D_{\frac{1}{2}}$ — 5p $^4S^0_{1\frac{1}{2}}$	
10H	2626.52	38061.9	$4p^4$ $^2P_{\frac{1}{2}}$ — 5p $^4P^0_{\frac{1}{2}}$	
3	2617.08	38199.9	5p $^4D^0_{2\frac{1}{2}}$ — 5d $^4F_{2\frac{1}{2}}$	
7h	2616.26	38211.1	5p $^4P^0_{\frac{1}{2}}$ — 11	
10H	2613.13	38256.9	5p $^4D^0_{3\frac{1}{2}}$ — 5d $^4D_{3\frac{1}{2}}$	
7H	2608.15	38329.9	5p $^4S^0_{1\frac{1}{2}}$ — 18	
9H	2606.20	38358.6	5p $^4D^0_{2\frac{1}{2}}$ — 5d $^4D_{2\frac{1}{2}}$	
3h	2601.58	38426.7	5p $^4P^0_{\frac{1}{2}}$ — 5d $^4P_{1\frac{1}{2}}$	
1H	2597.69	38484.3	5p $^2P^0_{1\frac{1}{2}}$ — 20	
8h	2595.98	38509.7	5p $^4D^0_{3\frac{1}{2}}$ — 5d $^4F_{3\frac{1}{2}}$	
6H	2594.48	38531.9	5p $^4D^0_{\frac{1}{2}}$ — 5d $^4D_{\frac{1}{2}}$	
10	2589.14	38611.3	5p $^4D^0_{1\frac{1}{2}}$ — 5d $^4D_{1\frac{1}{2}}$	
8h	2584.99	38673.3	5p $^4P^0_{2\frac{1}{2}}$ — 15	
6H	2573.17	38850.9	5p $^4D^0_{3\frac{1}{2}}$ — 13	
7H	2570.83	38886.3	5p $^4D^0_{1\frac{1}{2}}$ — 10	
2h	2565.22	38971.3	5p $^4D^0_{2\frac{1}{2}}$ — 11	
1	2554.21	39139.3	$4p^4$ $^2P_{1\frac{1}{2}}$ — 5p $^4P^0_{\frac{1}{2}}$	
7h	2551.09	39187.1	5p $^4P^0_{\frac{1}{2}}$ — 5d $^4P_{\frac{1}{2}}$	
			5p $^4D^0_{2\frac{1}{2}}$ — 5d $^4P_{1\frac{1}{2}}$	
7	2529.49	39251.8	$4p^4$ $^2P_{\frac{1}{2}}$ — 5p $^4P^0_{1\frac{1}{2}}$	
1h	2527.92	39546.3	5p $^4D^0_{\frac{1}{2}}$ — 10	?

TABLE II (*contd.*)

Intensity	λ(air)	ν(vac)	Classification	Remarks
1h	2524.43	39601.0	5p $^4D^0_{3\frac{1}{2}}-14$	
00	2513.08	39779.8	4d $^4F_{2\frac{1}{2}}-5p$ $^4S^0_{1\frac{1}{2}}$	
5	2497.43	40029.1	5p $^4P^0_{2\frac{1}{2}}-17$	
6	2482.60	40268.2	5p $^4D^0_{1\frac{1}{2}}-5d$ $^4F_{2\frac{1}{2}}$	
3h	2469.17	40487.2	5p $^4D_{2\frac{1}{2}}{}^0-12$	
6	2462.39	40598.7	$4p^4$ $^2P_{1\frac{1}{2}}-5P$ $^4P^0_{1\frac{1}{2}}$	
1bh	2450.44	40796.6	5p $^4P^0_{1\frac{1}{2}}-15$	
3h	2443.01	40920.7	5p $^4D^0_{2\frac{1}{2}}-5d$ $^4F_{3\frac{1}{2}}$	
4h	2435.76	41042.5	5p $^4D^0_{1\frac{1}{2}}-11$	
0h	2423.08	41257.3	5p $^4D^0_{1\frac{1}{2}}-5d$ $^4P_{1\frac{1}{2}}$	
1h	2422.71	41263.6	5p $^4D_{2\frac{1}{2}}{}^0-13$	
4b	2397.31	41700.7	5p $^4D^0_{\frac{1}{2}}-11$	
1	2396.07	41722.3	5p $^4P^0_{1\frac{1}{2}}-16$	
3	2379.48	42013.2	5p $^4D^0_{2\frac{1}{2}}-14$	
4	2378.73	42026.4	5p $^4D^0_{3\frac{1}{2}}-18$	
00	2375.50	42083.5	5p $^4D^0_{1\frac{1}{2}}-6s$ $^4P_{2\frac{1}{2}}$	
3	2371.63	42152.2	5p $^4P^0_{1\frac{1}{2}}-17$	
0	2365.79	42256.3	5p $^4P^0_{\frac{1}{2}}-15$	
0	2349.06	42557.2	5p $^4D^0_{1\frac{1}{2}}-12$	
4	2339.95	42722.8	$4p^4$ $^2P_{1\frac{1}{2}}-5p$ $^4P^0_{2\frac{1}{2}}$	
2	2326.41	42971.5	5p $^4S^0_{1\frac{1}{2}}-22$	
0	2323.96	43016.8	5p $^4D^0_{2\frac{1}{2}}-15$	
6	2313.29	43215.2	5p $^4D^0_{\frac{1}{2}}-12$	
0	2299.66	43471.3	5p $^4D^0_{3\frac{1}{2}}-19$	
8vbh	2293.44	43589.2	$4p^4$ $^2P_{\frac{1}{2}}-5p$ $^2D^0_{1\frac{1}{2}}$	
4	2292.27	43611.4	5p $^4P^0_{\frac{1}{2}}-17$	
1bh	2289.49	43664.4	5p $^4P^0_{1\frac{1}{2}}-19$	?
0	2274.94	43943.6	5p $^4D^0_{2\frac{1}{2}}-16$	
4	2270.02	44038.8	4d $^4F_{1\frac{1}{2}}-5p$ $^2P^0_{\frac{1}{2}}$	
1	2256.52	44302.3	5p $^4P^0_{1\frac{1}{2}}-20$	

TABLE II (*contd.*)

Intensity	λ(air)	ν(vac)	Classification	Remarks
0	2249.63	44437.9	5p $^4D^0_{2\frac{1}{2}}-18$	
1	2243.43	44560.7	5p $^4P^0_{1\frac{1}{2}}-21$	
00	2234.59	44737.0	5p $^4P^0_{2\frac{1}{2}}-22$	
00	2210.63	45221.8	$4p^4\ ^2P_{\frac{1}{2}}-5p\ \ ^2P^0_{\frac{1}{2}}$	
2	2184.55	45761.7	5p $^4P^0_{\frac{1}{2}}-20$	
3	2178.74	45883.7	5p $^4D^0_{2\frac{1}{2}}-19$	
2	2172.62	46012.9	5p $^4D^0_{1\frac{1}{2}}-16$	
0	2172.30	46019.7	5p $^4P^0_{\frac{1}{2}}-21$	
?	2153.68	46418.2	$4p^4\ ^2P_{1\frac{1}{2}}-5p\ \ ^2P^0_{1\frac{1}{2}}$	
?	2152.52	46442.5	5p $^4D^0_{1\frac{1}{2}}-17$	
4	2133.35	46859.8	5p $^4P^0_{1\frac{1}{2}}-22$	
3	2118.51 (vac)	47188.0	$4p^4\ ^2P_{1\frac{1}{2}}-5p\ \ ^2D^0_{2\frac{1}{2}}$	
2	1475.1	67790	$4p^4\ ^4P_{\frac{1}{2}}-5p\ \ ^4D^0_{\frac{1}{2}}$	
00	1434.7	69703	$4p^4\ ^4P_{1\frac{1}{2}}-5p\ \ ^4D^0_{1\frac{1}{2}}$	
5	1402.9	71283	$4p^4\ ^4P_{\frac{1}{2}}-5p\ \ ^4P^0_{\frac{1}{2}}$	
1	1393.0	71789	$4p^4\ ^4P_{1\frac{1}{2}}-5p\ \ ^4D^0_{2\frac{1}{2}}$	
2	1383.1	72303	$4p^4\ ^4P_{2\frac{1}{2}}-5p\ \ ^4D^0_{1\frac{1}{2}}$	
2	1351.4	73996	$4p^4\ ^4P_{1\frac{1}{2}}-5p\ \ ^4P^0_{1\frac{1}{2}}$	
1	1344.6	74374	$4p^4\ ^4P_{2\frac{1}{2}}-5p\ \ ^4D^0_{2\frac{1}{2}}$	
5	1313.5	76135	$4p^4\ ^4P_{1\frac{1}{2}}-5p\ \ ^4P^0_{2\frac{1}{2}}$	
1	1305.6	76591	$4p^4\ ^4P_{2\frac{1}{2}}-5p\ \ ^4P^0_{1\frac{1}{2}}$	
0	1304.9	76632	$4p^4\ ^4P_{\frac{1}{2}}-5p\ \ ^4S^0_{1\frac{1}{2}}$	Oxygen I
0	1303.7	76708	$4p^3\ ^2P^0_{1\frac{1}{2}}-4p^4\ \ ^4P_{\frac{1}{2}}$	
3	1302.2	76794	$4p^4\ ^4P_{2\frac{1}{2}}-5p\ \ ^4D^0_{3\frac{1}{2}}$	Oxygen I
1	1297.5	77074	$4p^3\ ^2P^0_{\frac{1}{2}}-4p^4\ \ ^4P_{1\frac{1}{2}}$	
0	1283.7	77903	$4p^4\ ^4P_{1\frac{1}{2}}-5p\ \ ^4S^0_{1\frac{1}{2}}$	
00	1272.8	78567	$4p^4\ ^4P_{\frac{1}{2}}-5p\ \ ^2P^0_{1\frac{1}{2}}$	
2	1270.3	78724	$4p^4\ ^4P_{2\frac{1}{2}}-5p\ \ ^4P^0_{2\frac{1}{2}}$	
3	1242.2	80500	$4p^4\ ^4P_{2\frac{1}{2}}-5p\ \ ^4S^0_{1\frac{1}{2}}$	
9	984.9	101532	$4p^3\ ^4S^0_{1\frac{1}{2}}-4p^4\ \ ^4P_{2\frac{1}{2}}$	

TABLE II (*contd.*)

Intensity	λ(vac)	ν(vac)	Classification	Remarks
8	960.4	104129	$4p^3\ {}^4S^0_{1\frac{1}{2}} - 4p^4\ {}^4P_{1\frac{1}{2}}$	
7	949.0	105380	$4p^3\ {}^4S^0_{1\frac{1}{2}} - 4p^4\ {}^4P_{\frac{1}{2}}$	
2	807.4	123856	$4p^3\ {}^2P^0_{\frac{1}{2}} - 5s\ {}^2P_{\frac{1}{2}}$	
0	805.7	124116	$4p^3\ {}^2P^0_{1\frac{1}{2}} - 4d\ {}^4P_{\frac{1}{2}}$	
5	798.8	125186	$4p^3\ {}^2P^0_{1\frac{1}{2}} - 5s\ {}^2P_{1\frac{1}{2}}$	
0	794.1	125926	$4p^3\ {}^2P^0_{\frac{1}{2}} - 3$	
00	788.7	126794	$4p^3\ {}^2P^0_{\frac{1}{2}} - 5s\ {}^2P_{1\frac{1}{2}}$	Br II
00	773.2	129339	$4p^3\ {}^2D^0_{2\frac{1}{2}} - 4d\ {}^4D_{2\frac{1}{2}}$	
3	768.8	130075	$4p^3\ {}^2D^0_{1\frac{1}{2}} - 4d\ {}^4D_{1\frac{1}{2}}$	
1	761.3	131361	$4p^3\ {}^2D^0_{2\frac{1}{2}} - 5s\ {}^4P_{1\frac{1}{2}}$	
2	759.9	131596	$4p^3\ {}^2P^0_{1\frac{1}{2}} - 5s'\ {}^2D_{2\frac{1}{2}}$	
3	754.5	132535	$4p^3\ {}^2P^0_{1\frac{1}{2}} - 5s'\ {}^2D_{1\frac{1}{2}}$	
1	746.6	133948	$4p^3\ {}^2D^0_{2\frac{1}{2}} - 5s\ {}^4P_{2\frac{1}{2}}$	
2	745.5	134142	$4p^3\ {}^2P^0_{\frac{1}{2}} - 5s'\ {}^2D_{1\frac{1}{2}}$	
2	740.8	134984	$4p^3\ {}^2P^0_{1\frac{1}{2}} - 4p^4\ {}^2D_{1\frac{1}{2}}$	
00	739.9	135150	$4p^3\ {}^2D^0_{1\frac{1}{2}} - 5s\ {}^4P_{2\frac{1}{2}}$	
6	736.4	135801	$4p^3\ {}^2D^0_{1\frac{1}{2}} - 5s\ {}^2P_{2\frac{1}{2}}$	
00	731.7	136674	$4p^3\ {}^2D^0_{2\frac{1}{2}} - 3$	
6	727.0	137546	$4p^3\ {}^2D^0_{2\frac{1}{2}} - 5s\ {}^2P_{1\frac{1}{2}}$	
00	720.8	138742	$4p^3\ {}^2D^0_{1\frac{1}{2}} - 5s\ {}^2P_{1\frac{1}{2}}$	
8	690.2	144890	$4p^3\ {}^2D^0_{2\frac{1}{2}} - 5s'\ {}^2D_{1\frac{1}{2}}$	
3	688.9	145153	$4p^3\ {}^2D^0_{1\frac{1}{2}} - 5s'\ {}^2D_{2\frac{1}{2}}$	
1	678.7	147351	$4p^3\ {}^2D^0_{2\frac{1}{2}} - 4p^4\ {}^2D_{1\frac{1}{2}}$	
6	677.8	147545	$4p^3\ {}^2D^0_{2\frac{1}{2}} - 4p^4\ {}^2D_{2\frac{1}{2}}$	
0	672.3	148741	$4p^3\ {}^2D^0_{1\frac{1}{2}} - 4p^4\ {}^2D_{2\frac{1}{2}}$	
6	620.4	161199	$4p^3\ {}^4S^0_{1\frac{1}{2}} - 5s'\ {}^2D_{1\frac{1}{2}}$	
9	611.1	163650	$4p^3\ {}^4S^0_{1\frac{1}{2}} - 4p^4\ {}^2D_{1\frac{1}{2}}$	

Attempts to locate the 6p levels with the help of the 6s ^1P intervals have led to the identification of the two levels 23° and 24°.

Using the Rydberg formula the absolute value of 5s $^1P_{2\frac{1}{2}}$ is obtained by Rao and Krishna Murty as 139269.0 cm^{-1} from the two members of the ns ^4P series.

This gives the limit 289529 cm^{-1} corresponding to a third ionisation potential of 35.89 volts. The calculation is verified and found correct. This is, therefore, adopted as the limit.

ACKNOWLEDGMENTS

The author is indebted to Prof. K. R. Rao for guidance throughout the progress of this work, which was done during the author's stay at the Andhra University, Waltair. He is thankful to Dr. K. Sreerama Murty and Dr. S. Paddi Reddy for their kind and constant help.

REFERENCES

Bhupala Rao, Y., 1956, *Ind. J. Phys.*, **30**, 371.
Bhupala Rao, Y, 1958, *Ind. J. Phys.*, **32**, 497.
Bloch, L. and Bloch, E., 1927, *Ann. de. Phys.*, **7**, 205.
Boyce, J. C., 1935, *Phys, Rev.*, **47**, 718.
Deb, S. C., 1930, *Proc. Roy. Soc. London.*, A**127**, 197.
Krishna Murty, S. G. and Rao, K. R., 1935, *Proc. Roy. Soc. London.*, A**149**, 56.
Lacroute, P., 1935, *Ann. de. Phys.*, **3**, 3.
Martin, D. C., 1935, *Phys. Rev.*, **48**, 938.
Meggers, W. F., Shenstone, A. G. and Moore, C. E., 1950, *Bur. Std. Jour., of Research* **45**, 346.
Moore, C. E., 1952, *Atomic Energy Levels, Vol. II.*
Rao, A. B., and Krishna Murty, S. G., 1939, *Proc. Phys. Soc.*, **51**, 772.
Rao, K. R., 1927, *Proc. Phys. Soc.*, **39**, 161.
Rao, K. R., 1944, *Curr. Sci.*, **13**, 72.
Rao, K. R., and Krishna Murty, S. G., 1937, *Proc. Roy. Soc. London.*, A**161**, 38.
Rao, K. R., and Badami, J. S., 1931, *Pric. Roy. Soc., London.*, A**131**, 154.

44

TOPOTACTIC TRANSFORMATIONS IN IRON OXIDES AND OXYHYDROXIDES*

D. R. DASGUPTA**

Indian Association for the Cultivation of Science,
Jadavpur, Calcutta-32

(*Received March* 26, 1961)

Plate VIII (A and B)

ABSTRACT. This paper records an investigation of the structures and chemical relations of iron oxides, hydroxides and oxyhydroxides. In the course of the work structural relations were also found between them which exemplified the new concept of topotaxy or change of composition of crystals occurring without any large discontinuity of structures. Starting with $Fe(OH)_2$ whose structure is built up of hexagonal close-packed hydroxyl layers, it is seen that when it decomposes into FeO there is an oriented relationship between the two phases. The [001] of $Fe(OH)_2$ becomes the [111] of cubic FeO and [110] of the former becomes [110] of the latter. Again, when $Fe(OH)_2$ is oxidised by strong H_2O_2 or $(NH_4)_2S_2O_8$ solution to δ FeO.OH, the arrangement of the close-packed layers changes from AcB to $A\frac{1}{2}cB\frac{1}{2}cA$, the directions of the axes remaining the same. As it was not possible to get any single crystals of green rusts, direct evidences about the oriented relationship between them and their transformation products could not be found. But the proposed structure for the green rusts definitely speaks in favour of the oriented relationships. The transformations of γ-FeO.OH to γ-Fe_2O_3 and then to α-Fe_2O_3 have been studied in great detail. It was found that the [100], [010] and [001] axes of γ-FeO.OH become [001],[110] and [1$\bar{1}$0] of γ-Fe_2O_3 after transformation. In the second transition from γ-Fe_2O_3 to α-Fe_2O_3, crystals of the latter grow with their [001] axes parallel to [111] of γ-Fe_2O_3 and their [1$\bar{1}$0] directions being parallel to [110] of γ-Fe_2O_3. The same sort of oriented relationship as in between γ-Fe_2O_3 and α-Fe_2O_3 was found in the transformation of Fe_3O_4 to α-Fe_2O_3. Several forms of γ-Fe_2O_3 prepared by various methods have also been studied by X-rays. The transformation of rhombohedral $FeCO_3$ to cubic FeO and Fe_3O_4 has also been found to have oriented relationship. The similarity of the structures of $FeCO_3$ and FeO suggested that the triad axis of $FeCO_3$ would be parallel to one of the triad axes of FeO and that the three diad axes of both phases were interchanged, FeO and Fe_3O_4 having parallel orientation to each other. The transformation of β-FeO.OH to α-Fe_2O_3 could not be explained in terms of oriented relationship. From the similarity of the powder patterns and also the comparison of intensities of the diffraction lines, it is thought that β-FeO.OH has a structure similar to Hollandite mineral (α-MnO_2).

INTRODUCTION

Up to the present time physico-chemical studies have shown the existence of three forms of iron oxyhydroxides referred to as α, β and γ-Fe_2O_3, H_2O or FeO.OH.

*This work was submitted as a part of the thesis for the Ph.D. degree of the University of London.

**At present Senior Mineralogist, Geological Survey of India, 29, Chowringhee, Cal-16.

Of the anhydrous oxides of iron, α-Fe_2O_3, γ-Fe_2O_3 and Fe_3O_4 can be obtained by dehydrating some of the oxyhydroxides (FeO.OH), by direct precipitation or by oxidation of $Fe(OH)_2$ with different types of oxidising agents. The remaining anhydrous oxide, FeO, may be obtained by decomposing $Fe(OH)_2$ or some organic ferrous salts in vacuo or in an inert atmosphere. Most of these hydrous and anhydrous oxides of iron can be found as natural minerals. Together with the study of various physical and chemical properties of these compounds, a number of methods have been found for preparing them synthetically. Welo and Baudisch (1925, 1933, 1935) reviewed all the work done on the iron oxides and oxyhydroxides up to that time and tried to draw up a general relationship between the different iron compounds. However, they themselves expressed doubts about the existence of some members in the iron oxide-oxyhydroxide system and also about the modes of transformation between the compounds. Although various methods of preparing the different oxides and oxyhydroxides and also how one can be obtained from the other are known, the structural inter-relationships among these compounds are quite unknown.

The structures of most of the oxides and oxyhydroxides of iron are built up of close-packed oxy/hydroxyl layers. It seems possible that when one form of iron oxides or oxyhydroxides transforms into another, the change may be effected simply by removing or adding close-packed oxy/hydroxyl layers from or to the original structures. Thus one might expect to find an oriented relationship between the original and transformed products. Such a relationship, which is not limited to any particular type of crystal, was observed by Goldsztanb (1931, 1935) in the transformation of α-FeO.OH to α-Fe_2O_3. This sort of relationship occurs frequently in metals and also in inorganic compounds. A striking example of this oriented relationship can be found in the case of cubic and hexagonal metallic cobalt crystals. There the basal hexagonal face becomes one of the {111} faces of the face-centred cubic form. Similarly, in the transformation between α and γ-iron, the {110} faces of the body-centred form becomes the close-packed {111} faces of the face-centred cubic form. All these changes mean that the main determining elements of the lattice do not change and the other elements only move from one symmetrical position to another in substantially the same cell. The minimum disturbances caused when the hydroxyl ions are removed as water molecules also suggest that the evidence of oriented relationship among the oxides and oxyhydroxides of iron may be found.

The best method of studying these oriented transformations is to make X-ray investigations on single crystals of different compounds before and after the transformation and also during it, if possible. If an oriented relationship exists, the diffraction photographs taken both before and after the transformation will show some common directions. When single crystals are not available, the powder diffraction method can provide indirect evidence. Sometimes, accord-

ing to the nature of transformation, a multiplicity of the reflections may correspond to a single direction from the original crystal. In this case, the similarities between the structure of the two phases may throw some light on any possible inter-relationship.

This sort of inter-relationship can be explained in terms of topotaxy, a term proposed by Gorter to denote the transformation from one crystalline phase to another, where there are definite oriented relationships between the axes of the original and transformed crystals. In general, the topotactic change consists of two parts, geometrical and chemical. The geometrical part classifies the way in which one lattice can be transformed into another while retaining the original network of the structure. The chemical part, on the other hand, accounts for the possibility of replacing one kind of atom by another and also the increase or lowering the total number of atoms per unit of lattice. True topotactic changes involve more than internal rearrangements of atoms along with the substitution, removal or addition of atoms to the original structure. In general, topotactic changes involving the loss or gain of atoms will leave the main symmetry directions of the crystals unchanged. But it also seems possible that an asymmetrical crystals may, by the loss of its atoms, transform into a form of higher symmetry. Further topotactic changes may occur on the newly formed crystals.

Thus with the aim of establishing what structural relationships exist between the different phases, most of iron oxides and oxyhydroxides and their transformations from one to the other have been studied in great detail. The results of the investigations are given in the next section.

EXPERIMENTAL RESULTS

(a) *Ferrous hydroxide* ($Fe(OH)_2$)

Thesn ow-white precipitate of $Fe(OH)_2$ which is obtained when an alkali is added to a ferrous salt solution, turns greenish as soon as it comes in contact with air. To show the true colour of $Fe(OH)_2$ precipitate, it is necessary to boil both the alkali and salt solution before mixing in order to eliminate the dissolved oxygen and the precipitation must be carried out in an inert atmosphere. Natta and Casazza (1928) from the powder diffraction photograph determined the structure of $Fe(OH)_2$. They found it to be hexagonal with one formula unit in the unit cell of axial parameters $a = 3.24$ Å and $c = 4.47$ Å. Thes tructure is built of two hexagonal close-packed OH' layers having Fe in the octahedral position in between them. The atomic coordinates are one Fe at (0,0,0) and two OH at $\pm(2/3, 1/3, Z)$ with $Z = 0.26$. It is to be noted here that the OH' layer has Fe^{++} on one side of it, whereas on the other side it is bound to another OH' layer by hydroxyl bonds.

Though it is thought that $Fe(OH)_2$ is very unstable at ordinary temperature and in contact with air, recent work by Shipko and Douglas (1956) had shown

that pure $Fe(OH)_2$, in contact with a solution of potassium chloride or excess of hydroxyl ion with complete exclusion of oxygen, was stable for a period of six months. Moreover, Gayer and Woonter (1957) reported from their chemical analysis that the green precipitate, observed at the initial stage of the oxidation of white $Fe(OH)_2$, no traces of ferric ions were found. Our (1960) work also showed that even when 20% of Fe^{++} ion in $Fe(OH)_2$ was oxidised to Fe^{+++}, there was no change in the structure of $Fe(OH)_2$.

When the white precipitate of $Fe(OH)_2$ is washed with oxygen free water and then heated to dryness it decomposes to FeO, some Fe_3O_4 also being formed at the same time. Recently, Goodman (1958) has shown from electron microscope and electron diffraction study of single crystal of $Mg(OH)_2$ that on dehydration of $Mg(OH)_2$ to MgO there is an oriented relationship between the two phases; the [001] of the hexagonal $Mg(OH)_2$ crystal transforms into [111] of the cubic MgO and the [110] of $Mg(OH)_2$ becomes [110] of MgO. As $Fe(OH)_2$ is very unstable, it was not possible to study the oriented relationship between $Fe(OH)_2$ and FeO using single crystal. From the fact that both $Mg(OH)_2$ and $Fe(OH)_2$ have the same structure (CdI_2 type) and also from the similarity between the MgO and FeO structure (NaCl type), it seems reasonable to think that in the transformation of $Fe(OH)_2 \rightarrow FeO$, the same type of oriented relationship occurs. Fig. 1 shows how two hydroxyl layers in $Fe(OH)_2$ could combine together to form a single

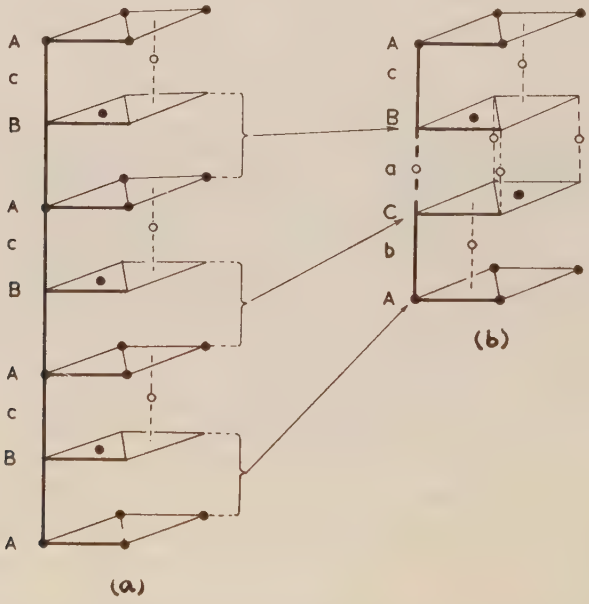

Fig. 1 Transformation of $Fe(OH)_2 \rightarrow FeO$.
(a) The arrangement of hydroxyl layers along [001] of $Fe(OH)_2$
(b) The arrangement of oxygen layers along [111] of FeO.

layer of oxygen in FeO. The oriented relationship which occurs between FeO and Fe_3O_4 has been discussed later on.

(b) *Delta ferric oxyhydroxide* (δ-FeO.OH)

$Fe(OH)_2$ in alkaline solution, when oxidised by air or oxygen, transforms into α-FeO.OH. The possibility of oriented relationship between $Fe(OH)_2$ and α-FeO.OH has been reported by Francombe and Rooksby (1959).

Glemser and Gwinner (1939) reported that $Fe(OH)_2$, when oxidised by H_2O_2 or $(NH_4)_2S_2O_8$ in excess, transformed into a ferromagnetic compound, which they called δ-Fe_2O_3. The X-ray photograph of this δ-Fe_2O_3 was interpreted by them in terms of a hexagonal cell with axial parameters $a = 5.09$ Å and $c = 4.41$ Å. This particular compound was studied by us in great detail and found not to be an anhydrous oxide of iron but an oxyhydroxide (FeO.OH). Moreover, the X-ray diffraction photograph was indexed in terms of a smaller hexagonal cell with $a = 2.941 \pm 0.005$ Å and $c = 4.49 \pm 0.01$ Å (Bernal, Dasgupta and Mackay, 1959).

Though stable at room temperature, δ-FeO.OH could not be obtained in the form of a single crystal. Hydrothermal treatment was attempted but it was found that when powdered δ-FeO.OH was heated in a bomb at 100°C, it was converted into α-Fe_2O_3. From the similarity of the powder pattern and axial parameters of δ-FeO.OH and $Fe(OH)_2$ and also from the fact that the pattern of δ-FeO.OH could be obtained from that of $\alpha-Fe_2O_3$ by choosing lines with l indices divisible by 3, it seems reasonable that the structure of δ-FeO.OH is intermediate between those of $Fe(OH)_2$ and α-Fe_2O_3. It should be pointed out here that in $Fe(OH)_2$, OH layers have Fe on one side of it, whereas on the other side they are connected to another OH layer by hydroxyl bonds. But in α-FO_2O_3, the hexagonal close-packed oxygen layers have Fe, in the octahedral sites, on both the sides. The striking feature of the powder pattern of δ-FeO.OH is the very weak (often absent) (001) reflection. This suggests that iron must be in the octahedral position on both sides of the close packed O′/OH′ layers. The density of δ-FeO.OH allows only one formula unit in the unit cell. The number of iron in the unit cell is thus one. To satisfy the condition for the 001 reflection, half of this iron should occupy the octahedral position on side of the closepacked layer, the other half being placed at the octahedral side on the other side of the layer. Fig. 2. shows the probable structure of δ-FeOH compared to that of $Fe(OH)_2$.

Feitknecht (1943) observed a similar type of structure for Cd(OH)F, where Cd^{++} ions are distributed equally between two octahedral sites between two hexagonal close-packed layers of mixed OH′ and F′ ions. However, in the case of δ-FeO.OH a better agreement between the observed and calculated intensities was found when 78% of the total iron was placed equally at the two octahedral sites (0,0,0; 0, 0, $\frac{1}{2}$) and the remaining part of iron in the four tetrahedral positions at $\pm$(1/3, 2/3, 1/8) and $\pm$(2/3, 1/3, 3/8).

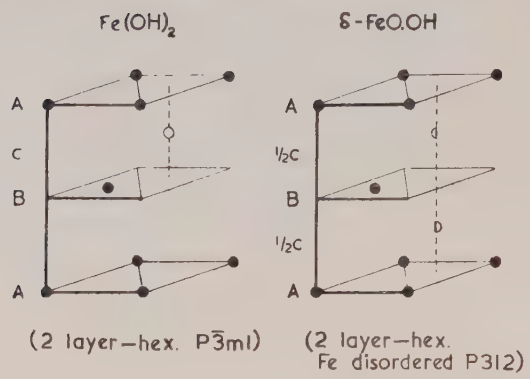

Fig. 2 Comparison of $Fe(OH)_2$ and δ-FeO.OH structure, the layers being shown along [001] axes.

(c) *The basic ferrous complexes*

When alkali insufficient to allow the complete precipitation of $Fe(OH)_2$, is added to ferrous salt solution a series of unstable complexes of ferrous salts are formed. Keller (1948) reported three basic chlorides obtained by partial precipitation from $FeCl_2$ with various concentrations of alkali. The basic complexes and their transformation on oxidation or dehydration have been studied by (1959). Of these complexes two are from $FeCl_2$ solution and the other from $FeSO_4$ solutions, are of great importance as they, on oxidation transform into γ-FeO.OH. These two complexes have been referred as green rust I and II respectively. The green rust I was found to belong to the hexagonal crystal system but the axial parameters varies for different preparations as follows :

(i) $a = 3.198 \pm 0.005$ Å, $c = 24.21 \pm 0.01$ Å from $FeCl_2$

(ii) $a = 3.23 \pm 0.01$ Å, $c = 22.50 \pm 0.01$ Å from $FeSO_4$

(iii) $a = 3.18 \pm 0.01$ Å, $c = 22.80 \pm 0.01$ Å from $FeBr_2$.

During oxidation green rust I, prepared from $FeSO_4$ solution, passed through another phase before being finally converted into γ-FeO.OH. This phase, termed as green rust II, also belongs to hexagonal crystal system with $a = 3.17 \pm 0.01$ Å and $c = 10.90 \pm 0.01$ Å.

Due to the instability of the green rusts it was not possible to make a complete study of their structures. However, from the dimensions of their axial lengths and the nature of the layer structures of almost all the oxides and hydroxides of iron some speculations can be made as to their structures in terms of the packing of equal spheres, if the following assumptions are made.

(i) Hexagonal layers of anions (O'' or OH'') are stacked so that regular tetrahedra fill the space. The layer distance is thus $0.817a$ where a is the diameter of the anion.

(ii) There will be empty tetrahedral and octahedral sites available for cations. There is no great distortion of the structure in filling these and the consideration is restricted only to the octahedral holes.

(iii) The sharing of faces by co-ordination octahedra (or tetrahedra) round the cation is rejected (Pauling's rule).

(iv) The compounds are all stoichiometric.

There are then only the following number of possibilities of stacking, where A, B, C denote the anions at (0, 0, Z); (1/3, 2/3, Z) and *a*, *b*, *c* denote the anions with the same co-ordinates.

(a) 2 *layers* : Composition AO_2; sequence of layers AcB—A ($c = 1.633a$ hexagonal)

(b) 3 *layers* : (i) composition AO; sequence of layers AcBaCbA (cubic $a = 1.414a$). (ii) composition A_2O_3, sequence of layers, AcBbC—A($c = 2.45a$ hexagonal), (iii) composition AO_3, sequence of layers AcB—C—A ($c = 2.45a$ hexagonal).

(*c*) 4 *layers*: composition A_2O_4, sequence of layers AcB—AbC—A or A—BcAbC—A ($c = 3.27a$ hexagonal).

(d) 6 *layers* : composition AO_2 sequence of layers AcB-cbA—BaC—A. ($c = 4.90a$, rhombohedral).

(*e*) 9 *layers* : composition A_2O_3; sequence of layers AcBaC—BaCbA—CbAcB—A (rhombohedral): composition AO_3: sequence of layers AcB—C—BaC—BaC—A—CbA—A or A—B—CaB—C—AbC—BcA ($c = 7.35a$, rhombohedral).

From the above considerations, it appears that as a first approximation the green rust I has the 9-layers rhombohedral structure ($c/a = 7.2$ observed) and green rust II has a 4-layers structure ($c/a = 3.4$ observed). Fig. 3 shows the possible structures of green rust I and II based on these assumptions.

(d) *α and γ-Ferric oxyhydroxides* (*α and γ*-FeO.OH)

These two oxyhydroxides of iron occur as natural mineral Goethite and Lepidiscite respectively. Synthetically, Goethite (α-FeO.OH) can be prepared by oxidising the green rusts. There are also other methods of preparation of these two oxyhydroxides synthetically.

α-FeO.OH transforms into α-Fe_2O_3 on dehydration. Goldsztaub (1931), while studying the transformation of single crystals of α-FeO.OH into α-Fe_2O_3, found an oriented relationship between them. He showed that the [100], [010] and [001] axes of the orthorhombic cell of α-FeO.OH transformed into [111], [110] and [112] axes respectively of the rhombohedral cell of α-Fe_2O_3.

γ-FeO.OH, on the other hand, transforms into γ-Fe_2O_3 dehydration and then to α-Fe_2O_3 on further heating. The transformation of γ-FeO.OH→γ-Fe_2O_3→α-Fe_2O_3 was studied by us (Bernal, Dasgupta and Mackay, 1957) using single

crystals of γ-FeO.OH. It was found that γ-Fe_2O_3 crystals are formed with their [001], [110] and [110] axes parallel to [100] [010] and [001] axes respectively of

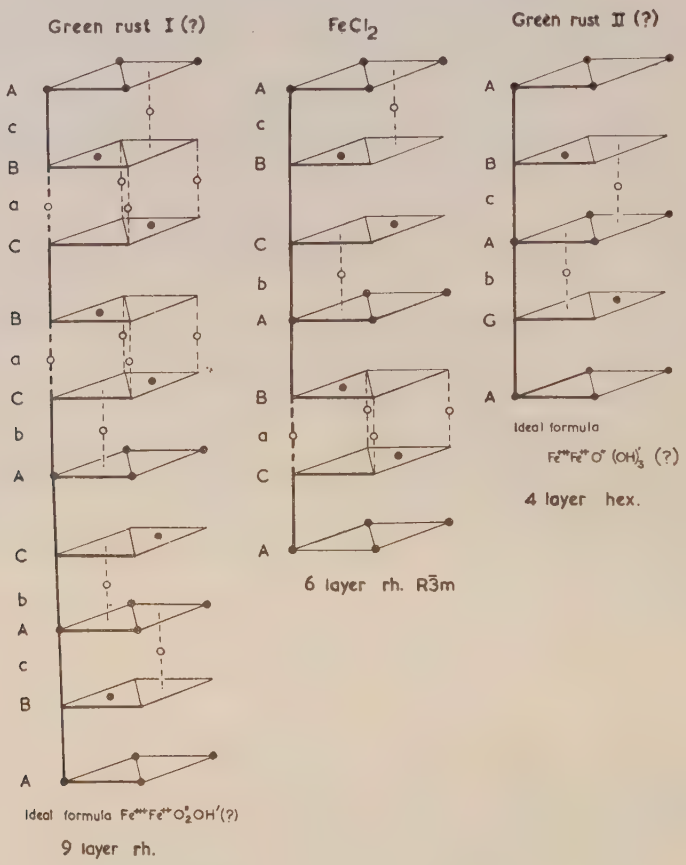

Fig. 3 Proposed structures of green rust I & II.

γ-FeO.OH. That the [100] of γ-FeO.OH is parallel to one of the cubic axes [001] of γ-Fe_2O_3 could be seen from the X-ray photograph (Plate VIIIA, Fig. 4(a)(b). In the second transition from γ-Fe_2O_3 to α-Fe_2O_3, crystals of the latter grow with their [001] axes parallel to [111] direction of α-Fe_2O_3 and their [110] directions being parallel to the [110] directions of α-Fe_2O_3 Fig. 6.

The mechanism of the transformation can be explained as follows. Fig. 7 shows the similarity between γ-FeO.OH and γ-Fe_2O_3 (spinel type) structures. The transition would require the removal of half of the hydroxyl group together with the hydrogen in the adjoining hydroxyl sheet, as water molecules. This is followed closing up of the (010) layers from 12.57Å to 8.85Å, that is, by 30% or 1.86Å per layer in the [010] direction of γ-FeO.OH. There is also a shift of half an

(a)

(b)

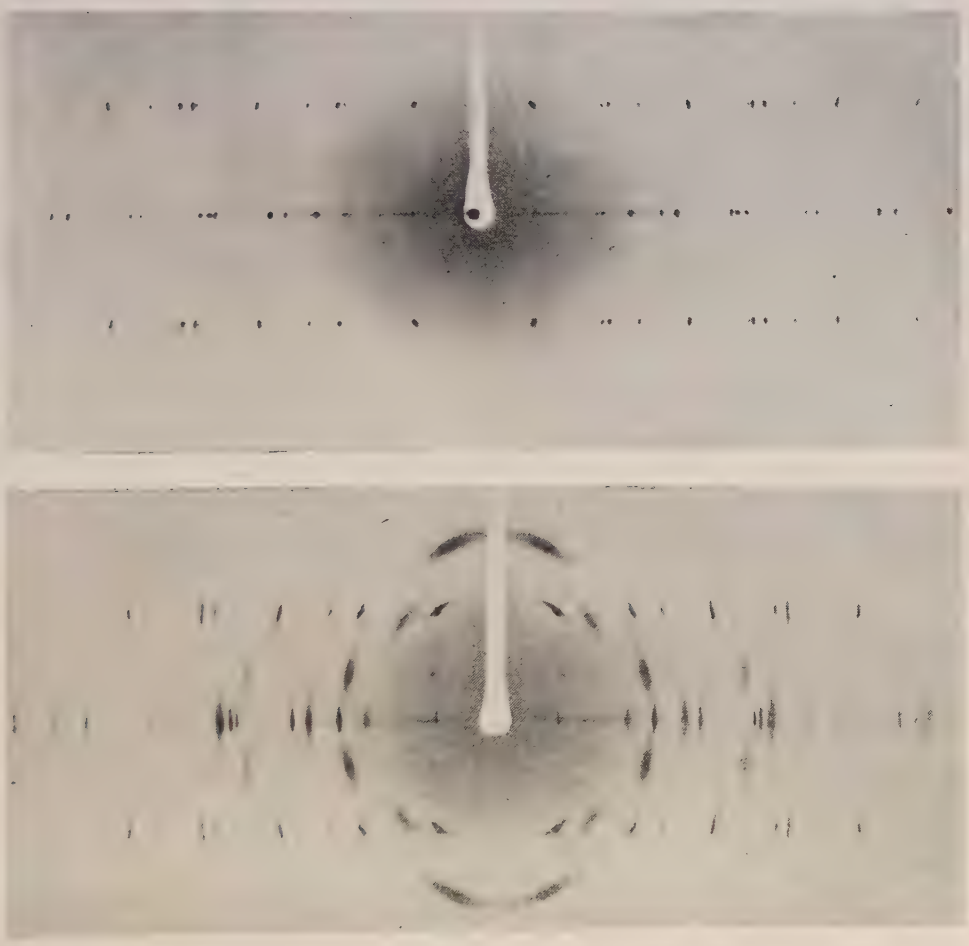

Fig. 4(a) Single crystal X-ray rotation photograph of γ-FeO taken along [100].
Fig. 4(b) Rotation photograph of a single crystal of γ-FeO.OH heated at 250°C for 3 hrs, showing the transformation γ-FeO.OH—γ-Fe_2O_3. The sharp spots correspond to unchanged γ-FeO.OH and the diffuse spots to γ-Fe_2O_3. The photograph was taken along the [100] axis of γ-Fe.OH and that corresponds to [001] axis of γ-Fe_2O_3.

(c)

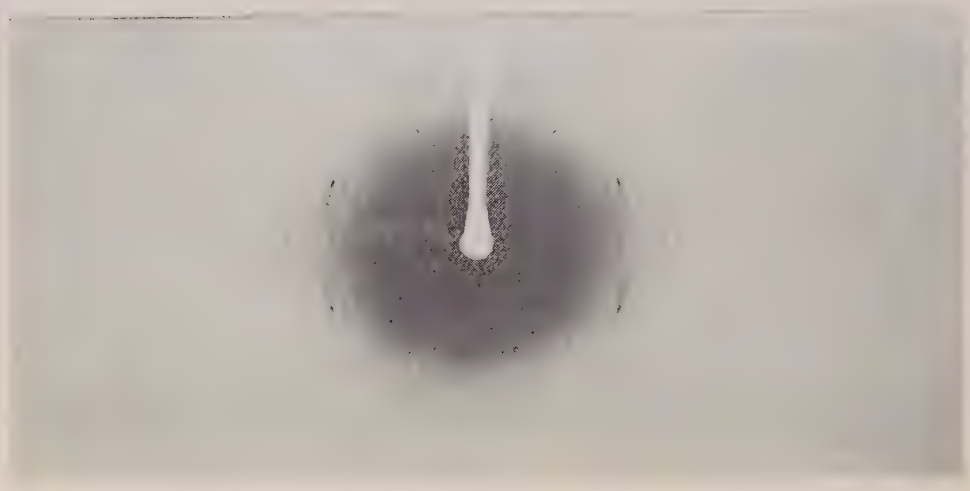

Fig. 4(c) Rotation photograph of single crystal of γ-FeO.OH heated to 250°C for 20 hrs showing the transformation of γ-Fe_2O_3—α-Fe_2O_3. The sharp spots are due to α-Fe_2O_3 and the diffuse spots are due to γ-Fe_2O_3.

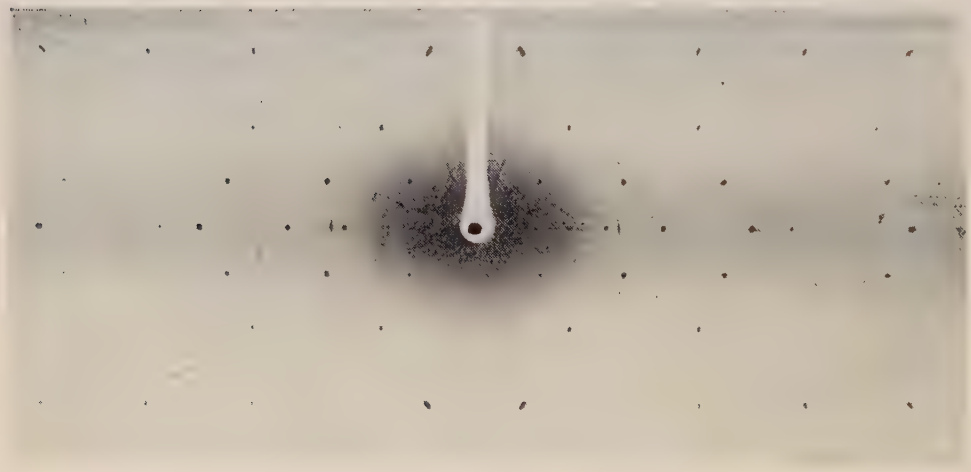

Fig. 5. Single crystal X-ray rotation photograph of Fe_3O_4 heated to 600°C for 26 hrs. taken along [100] of Fe_3O_4. The sharp spots are due to Fe_3O_4, while the weaker spots are due to γ-Fe_2O_3.

(a)

(b)

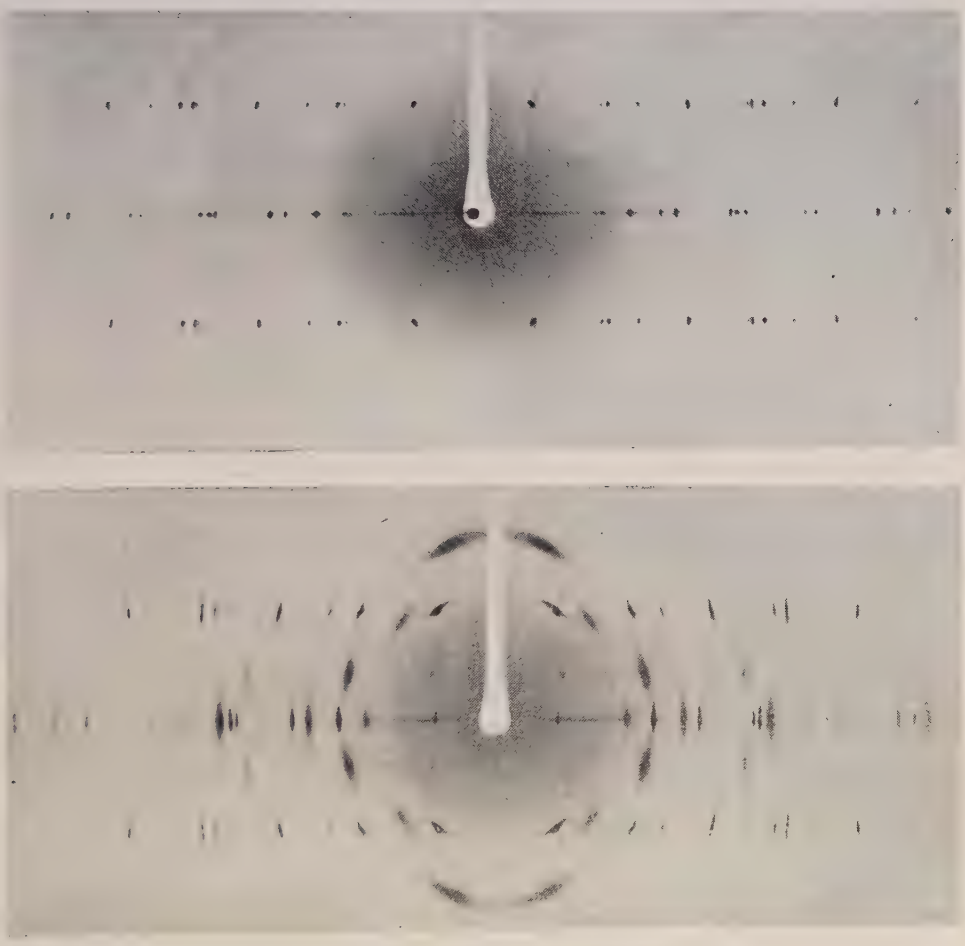

Fig. 4(a) Single crystal X-ray rotation photograph of γ-FeO taken along [100].
Fig. 4(b) Rotation photograph of a single crystal of γ-FeO.OH heated at 250°C for 3 hrs, showing the transformation γ-FeO.OH—γ-Fe_2O_3. The sharp spots correspond to unchanged γ-FeO.OH and the diffuse spots to γ-Fe_2O_3. The photograph was taken along the [100] axis of γ-Fe.OH and that corresponds to [001] axis of γ-Fe_2O_3.

(c)

Fig. 4(c) Rotation photograph of single crystal of γ-FeO.OH heated to 250°C for 20 hrs showing the transformation of γ-Fe_2O_3—α-Fe_2O_3. The sharp spots are due to α-Fe_2O_3 and the diffuse spots are due to γ-Fe_2O_3.

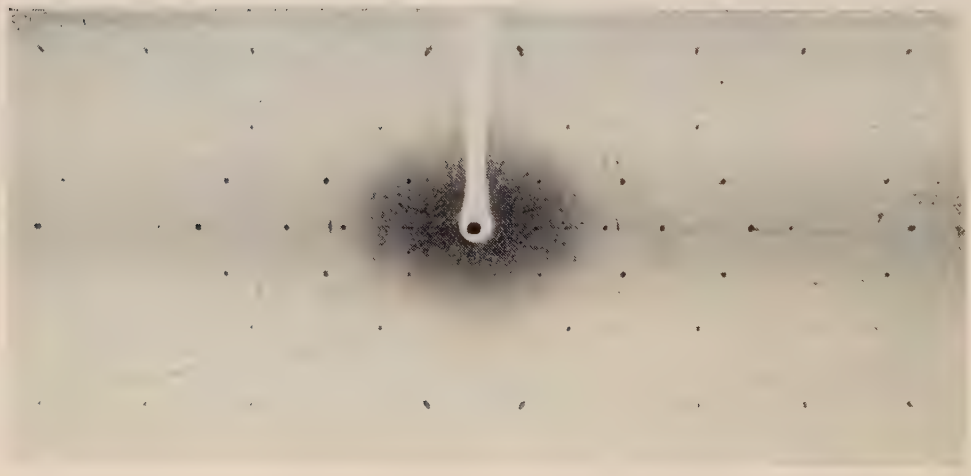

Fig. 5. Single crystal X-ray rotation photograph of Fe_3O_4 heated to 600°C for 26 hrs. taken along [100] of Fe_3O_4. The sharp spots are due to Fe_3O_4, while the weaker spots are due to γ-Fe_2O_3.

oxygen ion width (1.94 A) in the [100] direction. The resulting strain due to the shift may explain the disorder in the γ-Fe_2O_3 crystal (diffuseness of the spots). From the fact that the α-Fe_2O_3 crystals are oriented with respect to those of γ-Fe_2O_3 and not to those of γ-FeO.OH, it seems reasonable to think that the formation of α-Fe_2O_3 is subsequent to that of γ-Fe_2O_3. This transformation does not involve any loss or gain of material but only a restacking of close-packed oxygen atoms (cubic to hexagonal) on the {111} faces of γ-Fe_2O_3 (Fig. 6).

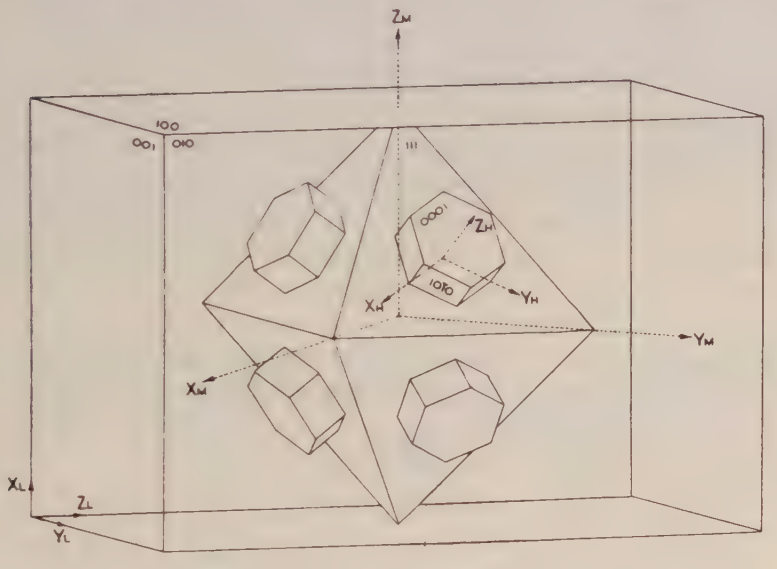

Fig. 6 Epitaxial relationship in the transformation γ-FeO.OH—γ-Fe_2O_3—α-Fe_2O_3.
Lepidocrocite Maghemite Haematite

(e) *Magnetite (Fe_3O_4) and Maghemite (γ-Fe_2O_3)*

The most important ferrite, Magnetite (Fe_3O_4), which may be written as $FeO.Fe_2O_3$, is the only certain oxide intermediate between ferrous and ferric oxides. Magnetite was known from very early ages to be one of the few ferromagnetic compounds as natural mineral. Magnetite which is cubic (face-centred) transforms into γ-Fe_2O_3 (cubic) on oxidation. γ-Fe_2O_3, on further heating, transforms into α-Fe_2O_3, (hexagonal). The transition of $Fe_3O_4 \rightarrow \gamma Fe_2O_3 \rightarrow \alpha Fe_2O_3$ brought up by heating magnetite in air has been studied by several workers. It was found that synthetic magnetite transformed more easily into γ-Fe_2O_3 than the natural magnetite. While oxidising synthetic magnetite, it was found that there are four forms of γ-Fe_2O_3. Three of them belong to the cubic system, while the other belong to the tetragonal system (Bernal, Dasgupta and Mackay, 1959; Van Oosterhout and Rooymans, 1958). The oxidation of Fe_3O_4 on heating has received considerable attention largely because of the difference in the behaviour of the natural and synthetic Fe_3O_4. Experimental

works of Schmidt and Vermaas (1955), Lepp (1957) and of many others showed that synthetic Fe_3O_4 oxidised first to γ—Fe_2O_3 and then to α-Fe_2O_3, whereas natural Fe_3O_4 oxidised only to α-Fe_2O_3 usually at a high temperature. Our X-ray study on the natural single crystal of Fe_3O_4 also confirmed this observation, Plate VIIIB, Fig. 5. The early workers found, on oxidation of Fe_3O_4 to γ-Fe_2O_3, that some extra lines appeared in the X-ray photographs, the general pattern remaining the same. It was found that those extra lines could be accounted for if γ-Fe_2O_3 had a primitive cell (Fe_3O_4 is face-centred cubic) of the approximate dimensions of Fe_3O_4. In recent years, various workers have expressed doubts about the structure of γ-Fe_2O_3, which was proposed by Thewlis (1931). Hagg (1953) from his X-ray diffraction study of γ-Fe_2O_3 concluded that the changes in the intensities of the diffraction lines and also in the density of γ-Fe_2O_3, from those of Fe_3O_4, were produced by the vacant sites in the iron atom lattice in the spinel phase rather than by the addition of oxygen. The suggested structure for γ-Fe_2O_3 was a defect spinel with cation vacancies in an oxygen ion frame work. Hence, when Fe_3O_4 is written as $Fe_8^{++}\ Fe_{16}^{+++}\ O_{32}^{--}$, γ-Fe_2O_3 can be written as $Fe^{+++}_{21\cdot33}\ \square_{2\cdot67}\ O_{32}^{--}$ where $\square_{2\cdot67}$ denotes cation vacancies. Verwey (1935) also suggested a similar structure where the vacancies were preferentially located at the octahedral sites

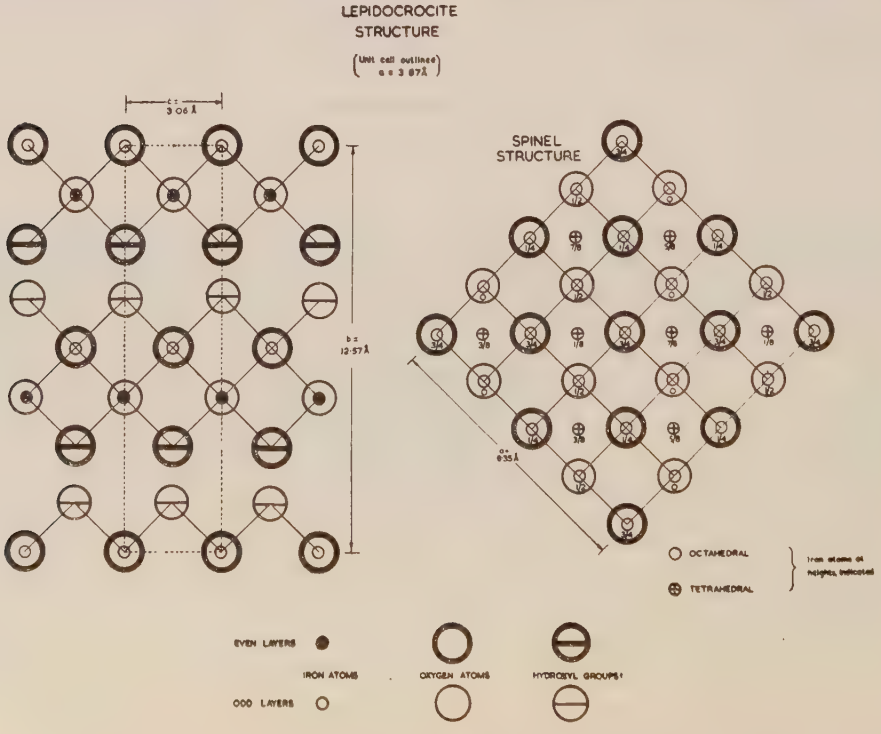

Fig. 7 Similarity of the γ-FeO.OH and γ-Fe_2O_3 (spinel) structures.

for Fe. This was supported by Henry and Boehm (1955) from their measurements of magnetic moment and also by Ferguson and Hass (1958) from their neutron diffraction study of γ-Fe_2O_3.

Since 1935, it has been generally accepted that γ-Fe_2O_3 is cubic with $10\frac{2}{3}$ molecules of γ-Fe_2O_3 in the unit cell. Van Oosterhout and Rooymanns (1958) have shown that in γ-Fe_2O_3, prepared by decomposing ferrous oxalate dihydrate in an atmosphere of steam and nitrogen followed by an oxidation at 250°C, some extralines appeared in the x-ray photographs. It has been possible for them to assign indices to all these extra lines using a tetragonal cell having $c = 3a$ with a same as that of the cubic cell. The new cell provides 32 molecules of γ-Fe_2O_3 instead of $10\frac{2}{3}$ in the cubic cell. It is seen that the structure of γ-Fe_2O_3 can be obtained from that of Fe_3O_4, when there is deficiency of Fe atoms in the octahedral sites of Fe_3O_4 structure. The relationship between Fe_3O_4 (or γ-Fe_2O_3)

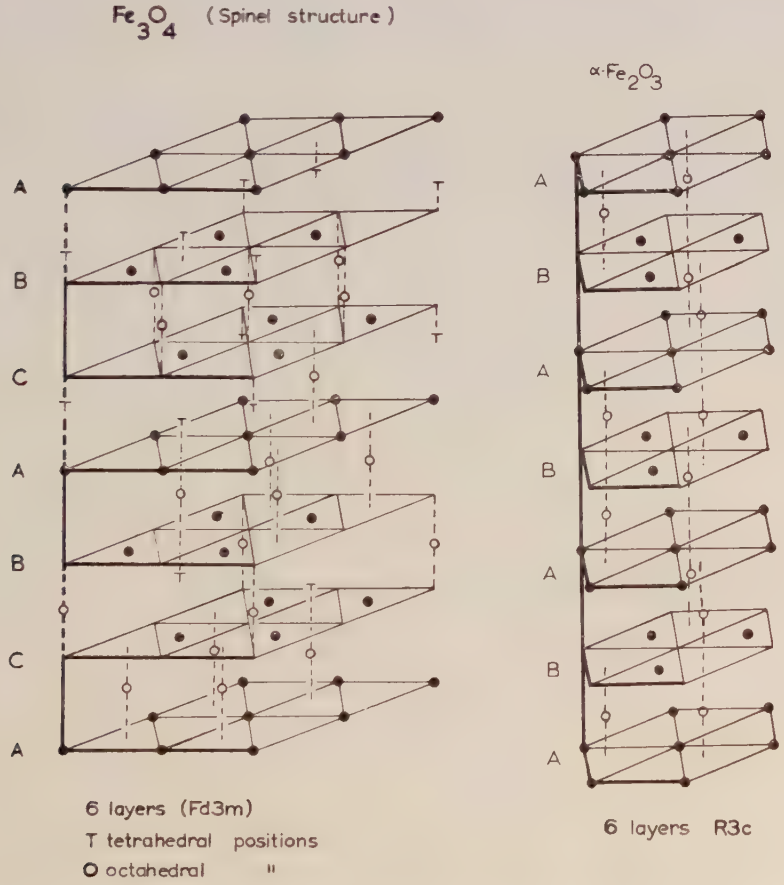

Fig. 8. Structural relationship between Fe_3O_4 and α-Fe_2O_3 along their [111] and [001] axes respectively.

and $\alpha-Fe_2O_3$ structures has already been explained earlier and is shown diagramatically in Fig. 8.

(f) *Siderite or $FeCO_3$.*

Though $FeCO_3$ does not fall in the iron oxide and oxyhydroxide series, yet it has been included in the present paper as it decompases into FeO and Fe_3O_4 when heated at high temperature.

Single crystal of $FeCO_3$ was heated in a sealed tube to 550°C. At that temperature it was not magnetic but on cooling it becomes highly magnetic. Though this magnetism was accompanied by a change of colour, the crystal retained its original sharp edged rhombohedral form. The faces of the crystal appeared to be very rough when viewed with a high power microscope. An X-ray photograph taken with the heated crystal rotating along the apparent [110] axis shows it to be transformed into FeO and Fe_3O_4, both of them having an oriented relationship with the original crystal. From the measurement of the X-ray photograph, it was seen that there was no unchanged $FeCO_3$ or Fe. The indices of the spots along the zero layer line shows that the cubic phases (FeO and Fe_3O_4) are oriented parallel to each other. The diad axis of the $FeCO_3$ crystal becomes one of the diad axes of FeO and Fe_3O_4. The oriented relationship between FeO and Fe_3O_4 can be easily understood from the similarity of their structures. (Fig. 9).

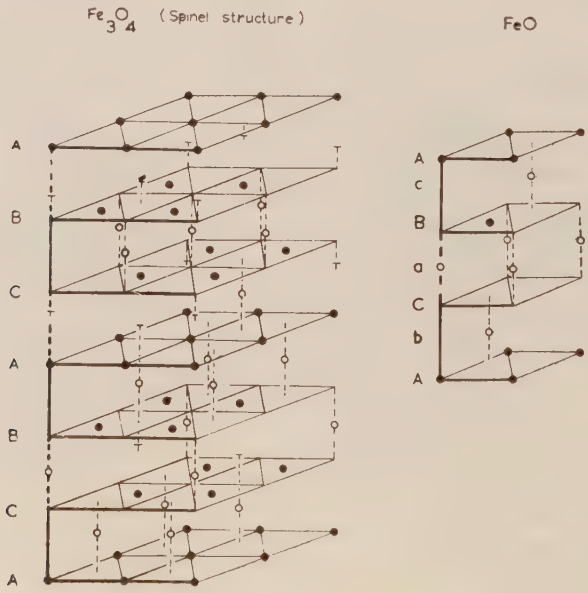

Fig. 9. Similarities between FeO and Fe_3O_4 structures showing the close-packed oxygen layers along the [111] directions.

The structure of $FeCO_3$ (rhombohedral), which is shown in Fig. 10, is not very different from those of NaCl or FeO. The FeO lattice compressed along [111]

axis would flatten out to become rhombohedral and make room for disc-shaped CO_3 ions in place of spherical O ions. So, it appears that FeO must derive from $FeCO_3$ simply by expulsion of CO_2 and change of angles between the sheet of atoms from 72° to 90°. The similarity also suggests that the triad axis of $FeCO_3$ will be parallel to one of the triad axes of the cubic crystal and that the three diad axes of both phases are interchanged. It is most remarkable that in spite of the loss of more than half of the oxygen atoms from the structure, the orientation is still preserved.

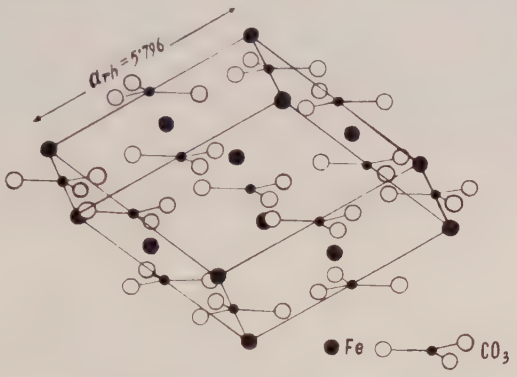

Fig. 10. structure of $FeCO_3$.

(g) *β-Ferric oxyhydroxide (β-FeO.OH)*

Weiser and Milligan (1935) reported this oxyhydroxide of iron. They found that when $FeCl_3$ was hydrolysed at 95°C for 6 hrs. the resultant brown precipitate was quite different from any of the existing oxides or oxyhydroxides of iron. From their dehydration isobar study, they concluded that it was a monohydrate of iron oxide (Fe_2O_3, H_2O or FeO.OH). In the present study it was found that not only $FeCl_3$, but FeF_3 and also any other ferric salts in presence of Cl' or F' ions gave β-FeO.OH on hydrolysis. Kratky and Nowotny (1938) tried to index all the lines of the powder diffraction pattern of β-FeO.OH in terms of an orthorhombic cell with $a = 10.46$ Å, $b = 10.24$ Å and $c = 2.34$ A. During the present investigation, it was found that all the lines in the powder photograph could be indexed in terms of a tetragonal cell with $a = 10.48 \pm 0.01$ Å and $c = 3.023 \pm 0.005$ Å. It will be worthwhile to mention here that no close pairs, such as (200, 020), (400, 040) where observed which could distinguish β-FeO.OH, as belonging to the orthorhombic crystal class.

As it was not possible to obtain any single crystals of β – FeO.OH, no detailed structure analysis could be carried out. Recently, Bystrom and Brystrom (1950) have determined the structure of the mineral hollandite and the related manganese oxide minerals. α-MnO_2 is tetragonal with $a = 9.8$Å and $c = 2.86$Å and Hollandite has a pseudotetragonal cell with $a = 9.96 \pm 0.05$Å and $c = 2.86 \pm 0.01$Å. The systematic absences in the case of hollandite are

the reflections with $h+k+l \neq 2n$. From the similarity of the powder pattern, axial lengths and the conditions for reflection (for β-FeO.OH, $h+k+l \neq 2n$), it seems that the two structures are similar. Fig. 11 shows the structure of Hollandite projected on (001). It can be seen that the metal ions are at the centre of the MO_6 octahedra and there are open channels parallel to c axis. In the case of Hollandite, Ba^{++} ions (its diameter being greater than the length of c axis) are distributed along these channels statistically. From the fact that the percentages of Cl^- or F^- ions, which are essential or the formation of β-FeO.OH, are not constant in β-FeO.OH, it is highly probable that in case of β-FeO.OH, also Cl′ or F′ ions enter the structure but are not present stoichiometrically. It appears that the Fe^{+++} ions, in the case of β-FeO.OH, should be at the centre of $Fe(O, OH)_6$ octahedra, whereas the Cl′ or F′ ions are distributed statistically along the channel parallel to the c axis.

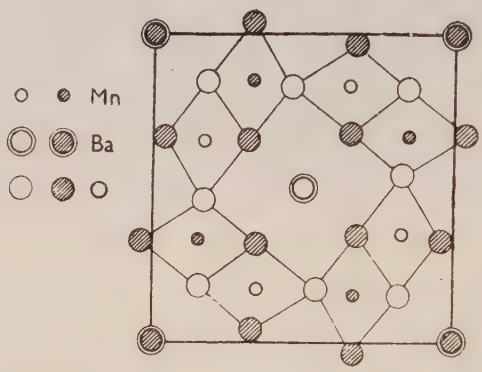

Fig. 11. Structure of Hollandite, open circles denote ions at $Z = 0$ and the filled circles at $Z = \frac{1}{2}$.

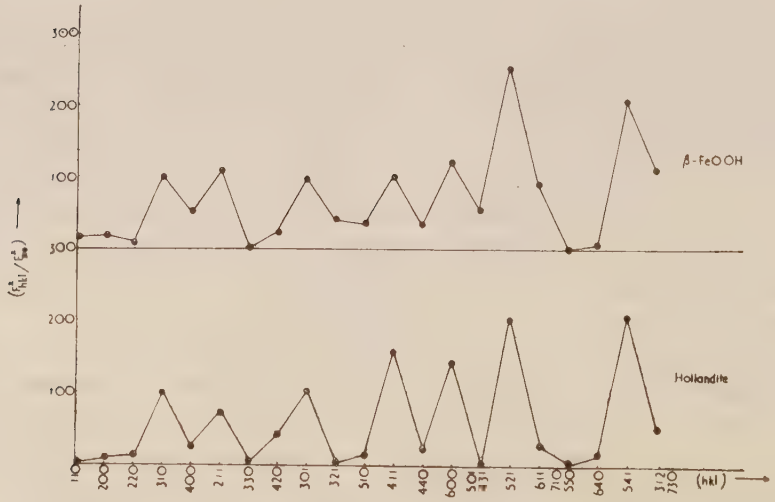

Fig. 12. Comparison of F^2_{hkl}/F^2_{31} values for Hollandite and β-FeO.OH.

The diameter of the Cl^- ion (3.62 Å) is greater than the *c* dimension of β-FeO.OH (3.023 ± 0.005 Å). This also suggests that Cl cannot be present in the structure stoichiometrically. The reason that β-FeO.OH could not be prepared from any ferric salt containing Br^- ions can be explained by the fact that the diameter of Br^- ion (3.90 Å) is too big for being placed along the *c* axis of β-FeO.OH. Moreover, the similarity between the curves for F^2_{hkl}/F^2_{310} ratio of Hollandite (calculated) and β-FeO.OH (observed), as shown in Fig. 12, also suggests a similarity between the two structures.

DISCUSSION

From the present study of iron oxides and hydroxides it seems quite evident that there are two definite series. The starting point of one series is the white $Fe(OH)_2$ and the basic ferrous salts, prepared by adding insufficient alkali, give rise to the other series. Most of the oxides and oxyhydroxides are the result of oxidation or dehydration of $Fe(OH)_2$. γ-FeO.OH, which could not be prepared from $Fe(OH)_2$ in any way, definitely belongs to the other series.

The formations and transformations of almost all the oxides and oxyhydroxides of iron can now be well represented by the Fig. 13. It is quite certain that all of them except β-FeO.OH are built up of close-packed oxygen layers and the nature of packing depends upon the structures of the individual phases. Fig. 13 shows the different form of transformations from one phase to another. As has been described in earlier chapters, the nature of all these transformations suggest that they take place, not by the complete breakdown of the structures of the origin phases but by simple shifting and re-stacking the different layers in the original structures. These observations naturally support the idea that whenever the steric conditions permit, solid state transformation, even if a large amount of the material is lost from the system, can proceed by a minimum rearrangement of the structures of the single crystals, involving little more than the mechanisms of dislocation glides, such as producing stacking faults and twinning.

The most interesting feature of the different members of the iron oxides and hydroxides groups is that most of them are built up of hexagonal close-packed or cubic close-packed layers of oxygen and hydroxyl ions. The sequences of the layers may be represented by ABABAB...or ABCABCABC... respectively. In some cases, some slight variations in the stacking of layers other than the conventional ones are possible.

$Fe(OH)_2$ is built up of hexagonal close-packed layers, the sequence of the layers being AcB-AcB, where the capital letters denote the positions of the anions and the small letters denote the position of the cation. When it changes into δ-FeO.OH, on oxidation by strong oxident, there is no substantial change in the arrangement of layers. As it can be seen from the proposed structure for δ-

FeO.OH, the arrangement of layers is the same as that of $Fe(OH)_2$. The difference in the two structures is that in δ-FeO.OH the one H ion must leave the lattice and

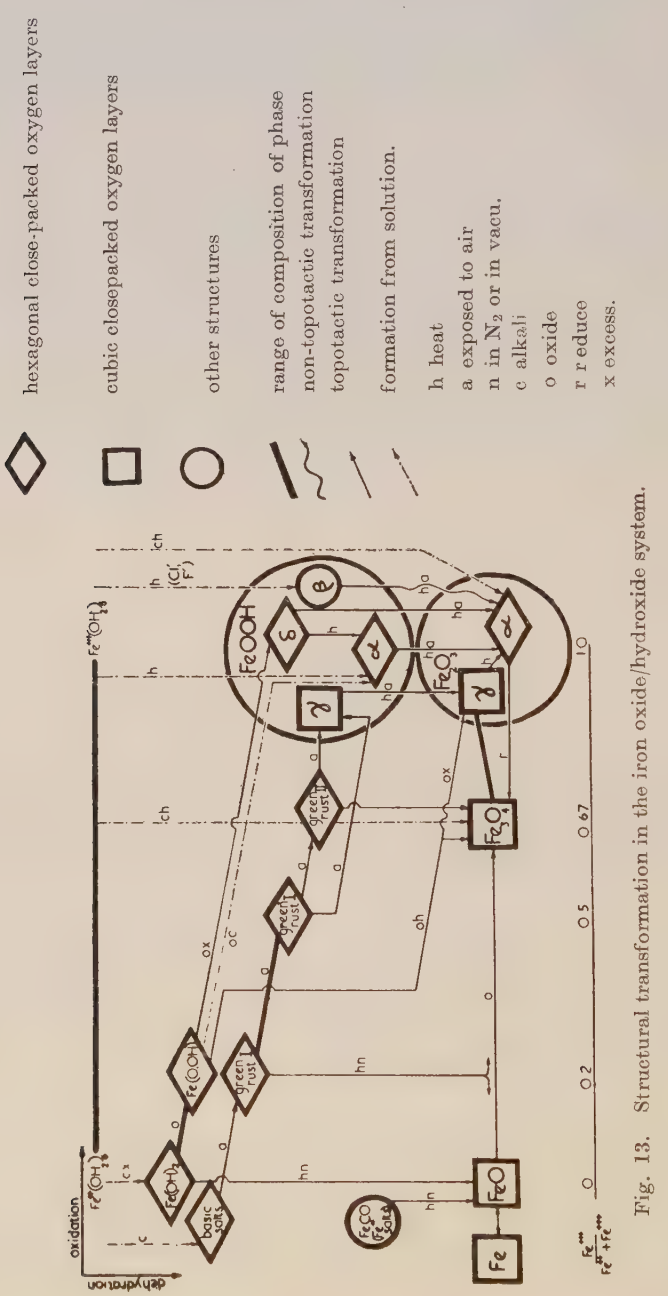

Fig. 13. Structural transformation in the iron oxide/hydroxide system.

the iron ion is divided into two parts so that the two octahedral positions between the oxygen and hydroxyl layers may be occupied. Thus, from the sequence AcB-AcB in $Fe(OH)_2$ it changes into $A\frac{1}{2}cB\frac{1}{2}cA\ldots$ in δ-FeO.OH. Again, in the transformation of $Fe(OH)_2 \rightarrow FeO$, it can be seen that the two hydroxyl layers in the former give up hydrogen in the form of water and form a single layer of oxygen in FeO. Here the hexagonal close-packed layers in $Fe(OH)_2$ transform into cubic close-packed layers in FeO, the original [001] axis of $Fe(OH)_2$ becoming the [111] axis of FeO. The transformation of $FeO \rightarrow Fe_3O_4$ can also be explained in terms of topotaxy. The addition of extra oxygen to FeO does not make any substantial change in the original structure so far as the stacking of the oxygen layers except changing the axial lengths (the axial lengths of Fe_3O_4 are nearly double those of FeO). The directions of the principal axes remain the same after transformation into Fe_3O_4. Though all the transformations such as $Fe(OH)_2 \rightarrow \delta$-FeO.OH. $Fe(OH)_2 \rightarrow$ FeO and $FeO \rightarrow Fe_3O_4$ can be explained in terms of topotaxy, it is not yet known how $Fe(OH)_2$ can convert directly into Fe_3O_4 on oxidation. If FeO were found in between $Fe(OH)_2$ and Fe_3O_4, then it would have been possible to describe the whole transformation as topotactic.

That two topotactic transformations can take place one after another was clearly illustrated by the transformation of a single crystal of Lepidocrocite (γ-FeO.OH) into Maghemite (γ-Fe_2O_3) and then into Hematite (α-Fe_2O_3). Lepidocrocite is built up of nearly cubic close-packed oxygen-hydroxyl layers, but their cubic faces are arranged at approximately 45° to the *c*-axis. When it is heated, one of the two adjoining hydroxyl layers is removed as water, converting the two layers into a single layer of oxygen only. The whole arrangement of the atoms then corresponds to a spinel structure (maghemite) having an oriented relationship with the original structure. When this transformed crystal is heated further, further change takes place. On the (111) faces of the freshly prepared Maghemite (transformed from γ-FeO.OH) the Hematite crystals grow up beautifully. Here, the [111] axis of the Maghemite becomes the [001] axis of the hematite crystals. The sequence of the oxygen layers is ABCABC in γ-Fe_2O_3, and ABABAB in α-Fe_2O_3, maghemite being cubic and hematite rhombohedral. There is also another interesting point to note in this transformation. In the X-ray photographs, the spots due to Maghemite are diffuse, whereas the spots due to Hematite are fairly sharp. The diffuseness of the maghemite spots indicates the change from an asymmetrical arrangement of the oxy-hydroxyl layers in γ-FeO.OH to a more symmetrical arrangement of oxygen layers in γ-Fe_2O_3. The more exact fit between Maghemite and Hematite, which permits easy recrystallisation, accounts for the sharpness of the Hematite spots. The Maghemite-Hematite transformation is very close to that which occurs in the Magnetite-Ilmenite transformation found in natural minerals. Here the original titaniferrous Magnetite breaks down into Ilmenite ($FeTiO_3$), the structure of which is similar to that of Hematite (α-Fe_2O_3).

As in the former transformation, here also the c-axis of Ilmenite becomes parallel to the [111] axis of Magnetite.

Some irregular arrangements of the oxy-hydroxyl layers other than the conventional ones, can be seen in the green rust I and II. In green rust I the arrangement of the layers is AB′CBC′ACA′B, whereas in II it is like A′BACA′BAC. Both these green rusts contain blocks of cubic and hexagonal close-packed layers. The cubic and hexagonal portions are ABC and BCB respectively in green rust I and BAC and ABA respectively in green rust II. Though the transformation of these two green rusts into μ-γ-FeO.OH or to FeO could not be demonstrated using single crystals, it appears that both the transformations are topotactic. Indirect evidence that the change is topotatic is provided by the fact that the green rusts I and II always give rise to cubic close-packed oxides or hydroxides. It can be seen that by suppressing one layer in three of the green rust I and one layer in every four in green rust II, as shown by the dashed letters, both the rusts transform into cubic close-packed structures, with the stacking of layers as ACBACB...and BACBAC... in green rust I and II respectively, whereas the direct oxidation of the hexagonal close-packed $Fe(OH)_2$ leads to two hexagonal close-packed oxyhydroxides, depending upon the nature and rate of oxidation.

A topotactic change involving the loss of atoms at one state and a gain of atoms at the next stage is also clearly illustrated in the transformation of $FeCO_3 \rightarrow FeO \rightarrow Fe_3O_4$. In the first stage CO_2 leaves the original structure; in the second stage oxygen enters into the lattice. This removal and the addition of atoms did not prevent a topotactic transformation.

It is now clear that most of the reactions shown in Fig. 13 can be expected to take place with oriented relationships between the original and the transformed phases. The exception is β-FeO.OH$\rightarrow\alpha$-Fe_2O_3. There is no similarity between the structures of β-FeO.OH and α-Fe_2O_3; on dehydration, the structure of β-FeO.OH breaks down completely and renucleation is needed for the transformation process.

ACKNOWLEDGMENTS

The work reported in this paper was a part of a research on the structures and properties of substances of geomagnetic interest carried out (in Birkbeck College Research Laboratory, London) under the guidance of Prof. J. D. Bernal, M.A., F.R.S., to whom the author is very much indebted. He is very grateful to his colleague Dr. A. L. Macky for his valuable suggestions and criticism during the progress of the work. Thanks are also due to Prof. K. Banerjee, D.Sc., F.N.I., who had kindly gone through the manuscript of this paper and given valuable suggestions.

REFERENCES

Bernal, J. D., Dasgupta, D. R., and Mackay, A. L., 1957, *Nature*, **180**, 645.

Bernal, J. D., Dasgupta, D. R. and Mackay, A. L., 1959, *Clay Min. Bull*, **4**, 15.

Bystrom, A. and Bystrom, A. M., 1950, *Acta Cryst.*, **3**, 146.

Dasgupta, D. R., 1955, *Proc. Nat. Inst. Sci. Ind.* **21A** 338.

Dasgupta, D. R., and Mackay, A. L., 1959, *Jour. Phys. Soc. Japan*. **14**, 932.

Feitknecht, W. and Bucher, H., 1943, *Helv. Chim. Acta.*, **26**, 2177.

Ferguson, G. A. and Hass, M., 1958, *Phys. Rev.*, **112**, 1130.

Glemser, O. and Gwinner, E., 1939, *Z. Anorg. Chem.*, **240**, 163.

Goldsztaub, S., 1931, *Compt. Rend.*, **193**, 533.

Goodman, J. F., 1958, *Proc. Roy. Soc.*, **A247**, 345.

Goldsztaub, S., 1935, *Bull. Soc. Franc. Min.*, **58**, 6.

Hagg, G., 1953, *Z. Krist.*, **B29**, 95.

Henry, W. E. and Boehm, M. J, 1956, *Phys. Rev.*, **101**, 1253.

Keller, G., Thesis, 1948, Bern University.

Kratky, O. and Nowotny, H., 1938, *Zeit. Krist.*, **A100**, 356.

Leep, H., 1957, *Amer. Min.*, **42**, 679.

Natta, G. and Casazza, A., 1928, *Gazz. Chim. ital.*, **58**, 344.

Schmidt, E. R. and Vermaas, F. H. S., 1955, *Amer. Min.*, 40, 422.

Thewlis, J., 1931, *Phil. Mag.*, 12, 1089.

Von Ossterhout, G. W. and Rooymans, C. J. M., 1958, *Nature*, **181**, 44.

Welo, L. A. and Baudisch, O., 1933, *Naturwissenschaften*, **21**, 659.

Welo, L. A. and Baudisch, O., 1925, *Phil. Mag.*, **50**, 399.

Weiser, H. B. and Milligan, W. O., 1935, *J. Phys. Chem.* **39**, 25.

Weiser, H. B. and Milligan, W. O., 1935, *J. Amer. Chem Soc.*, **57**, 238.

45

ON THE ELECTRONIC SPECTRA OF 2-AMINOPYRIDINE AND 3-AMINOPYRIDINE IN DIFFERENT STATES AND IN SOLUTIONS*

T. N. MISRA

Optics Department,

Indian Association for the Cultivation of Science,

Calcutta-32

(*Received June* 22, 1961)

Plate IX

ABSTRACT. The ultraviolet absorption spectra of 2-amino- and 3-aminopyridine in different states and also of their solutions in alcohol and *n*-hexane have been photographed and analysed. In the vapour phase, both the substances exhibit two systems of discrete bands due to $n \rightarrow \pi^*$ transition and $\pi \rightarrow \pi^*$ transition respectively. In the case of 2-aminopyridine in the liquid state and in solution, the system due to $\pi \rightarrow \pi^*$ transition shifts towards longer wavelengths so that the bands due to the $n \rightarrow \pi^*$ transition are not observed due to superposition of the two systems on each other. In the case of the solid state at the room temperature and also at —180°C, the spectrum seems to consist of two parts just separated from each other, the first part being the $\pi \rightarrow \pi^*$ system, which is shifted towards red by 3740 cm^{-1} and the second part is exactly in the same region in which the bands due to $n \rightarrow \pi^*$ transition in the vapour appear. In the case of 3-aminopyridine, the bands due to $n \rightarrow \pi^*$ transition is observed in the spectrum due to its solution in *n*-hexane, but no conclusion could be drawn regarding the presence or absence of $n \rightarrow \pi^*$ transition in the cases of solution in alcohol and pure liquid and also in the case of the solid at the room temperature and at —180°C owing to the superposition of the two systems.

It has been pointed out that the large shifts observed with the liquefaction of the vapour may be due to strong association of the molecules in the liquid state. There is also an increase in the width of the region of absorption with solidification of 3-aminopyridine and this has been attributed to the influence of neighbouring polar molecules in the crystal on the transition moment.

INTRODUCTION

It was first pointed out by Stephenson (1954) that near ultraviolet absorption spectrum of 3-bromopyridine in solution in iso-octane consists of two systems of bands due to $n \rightarrow \pi^*$ and $\pi \rightarrow \pi^*$ transitions, while in the case of 2-bromopyridine either in the solution or in the vapour state the former system is absent. It was also observed recently by the present author (Misra, 1960) that the spectrum of 3-bromopyridine in the vapour state consists of two systems of bands arising out

*Communicated by Professor S. C. Sirkar

of $n \rightarrow \pi^*$ and $\pi \rightarrow \pi^*$ transitions and in the spectrum of 2-bromopyridine in the vapour state the $n \rightarrow \pi^*$ transition is absent. As pointed out by Stephenson (1954), this is due to the inductive influence of the halogen atom on the sp^2 electron of the adjacent nitrogen atom. It was observed further (Misra, 1960) that in the case of 3-bromopyridine in the liquid state and in the solid state at -180°C, the $n \rightarrow \pi^*$ transition is absent and this was explained to be due to formation of associated groups through the non-bonding electron of the nitrogen atom and the hydrogen atom of the neighbouring molecules. The $n \rightarrow \pi^*$ transition was also found to be absent in the spectra due to solutions in alcohol because of formation of hydrogen bond through the sp^2 electron of the nitrogen atom of the pyridine ring and the OH group of the alcohol molecule. Similar conclusions were also drawn in the cases of pyridine and other substituted pyridines by Stephenson (1954), Banerjee (1956, 1957) and Roy (1958).

The ultraviolet absorption spectra of 2-amino and 3-aminopyridine in the vapour state did not appear to have been studied by any earlier worker and therefore, the influence of the NH_2 group on such $n \rightarrow \pi^*$ transition was not known. The present investigation was undertaken to analyse the absorption spectra of these two substances in the vapour state and also to study the influence of substitution of NH_2 group in place of the Br atom in the 2- and 3-position of the pyridine ring on the absorption spectra.

The absorption spectra of these two compounds in the liquid state, in the solid state at the room temperature and at -180°C and in solutions in different solvents have also been investigated in order to study the influence of different environments on the two transitions mentioned above.

EXPERIMENTAL

Chemically pure samples of 2-aminopyridine and 3-aminopyridine supplied by Fluka, Switzerland were fractionated and the proper fractions were distilled under reduced pressure just before use. Cells of length 50 cm, 25 cm and 10 cm were used to study the spectra due to the vapours. The absorption cell was filled up with the vapour at saturation vapour pressures at different temperatures. Two separate electrical heaters, one for the absorption cell and the other for the bulb containing the liquid and attached to the absorption cell, were used to control the temperature. The bulb containing the liquid was always kept at a temperature about 10°C lower than that at any part of the absorption cell.

To produce low pressures in the vapour in the absorption tube, the reservoir containing the liquid was immersed in suitable low temperature baths while the tube was left at the room temperature.

With an absorption cell of length 25 cm, the bulb containing the compound was kept at 35°C to record both the $n \rightarrow \pi^*$ and $\pi \rightarrow \pi^*$ system of 2-aminopyridine.

A 50 cm long absorption cell with the reservoir at 60°C was needed to record the bands due to the $n \rightarrow \pi^*$ and $\pi \rightarrow \pi^*$ transitions in 3-aminopyridine. The temperature of the bulb was raised to 70°C to record the $n \rightarrow \pi^*$ system distinctly.

Very thin films of thickness of the order of a few microns of the substances were required to produce the absorption bands in the solid state. To study the spectra in the liquid state, the thin films of the substances enclosed between two quartz plates were placed in a heating chamber which was kept at temperatures about 5°C above the respective melting points of the substances.

The solvents used to study the absorption spectra of the substances in the solutions were ethyl alcohol and *n*-hexane. The solvents were found to produce no absorption bands in the region under consideration. A brass cell of thickness 1 cm provided with quartz window was used for the solutions and the strength of the solution for each compound was about .01% by weight.

Spectrograms were taken on Agfa Isopan films backed by a metal sheet with a Hilger E 1 spectrograph giving a dispersion of the order of 3A per mm in the region of 2600 Å. Iron arc spectrum was photographed on each spectrogram as a comparison.

Microphotometric records were taken with a Kipp and Zonen self-recording microphotometer. The absorption spectra were calibrated with the help of microphotometric records of the iron lines using the method described in an earlier paper (Sirkar and Misra, 1959). As the infrared absorption spectra of these substances had not been studied thoroughly by previous workers, the infrared absorption spectra of solution of 2-aminopyridine in CCl_4 and that of 3-aminipyridine in chloroform were recorded with a Perkin Elmer Model 21 spectrophotometer using rocksalt optics in order to find out the ground state vibrational frequencies and these were utilised to check the excited state frequencies obtained from the ultraviolet absorption spectra.

RESULTS AND DISCUSSIONS

2-*Aminopyridine*

Microphotometric records of the absorption spectra of 2-aminopyridine in different states and in solution in different solvents are reproduced in Figs. 1—3, and the spectrum of the substance in the vapour phase is reproduced in Plate IX, Fig. 4(a). The wave numbers of the bands in cm^{-1} with their approximate strengths and probable assignments are given in Tables I-III.

(a) *Spectrum of the vapour phase* :

It can be seen from Fig. 1 that the absorption spectrum of 2-aminopyridine in the vapour phase shows two distinct systems of bands. One of these two systems (Transition I) consisting of sharp, narrow line-like bands starts from

about 32700 cm^{-1} and extends to the region of the other system which consists of broad bands resembling those due to other substituted benzenes. The former system has been attributed to the $n \rightarrow \pi^*$ transition after Kasha (1950) and the latter to the $\pi \rightarrow \pi^*$ transition. The analysis of the bands of these two systems is discussed separately in the following sections.

TABLE I

Ultraviolet absorption bands of 2-aminopyridine in the vapour phase

Transition I		Transition II	
wave number (cm^{-1}) and strength	Assignment	Wave number (cm^{-1}) and strength	Assignment
32885 (w)	0 — 564	34324 (s)	0,0
32999 (w)	0 — 455	34618 (w)	0 + 294
33070 (w)	0 — 379	34796 (s)	0 + 472
33157 (w)	0 — 292	34987 (m)	0 + 663
33223 (w)	0 — 226	35250 (s)	0 + 926
33364 (m)	0 + 210 — 292	35559 (s)	0 + 1235
33449 (vs)	0,0	35765 (s)	0 + 1441
33519 (w)	0 + 525 — 455	36025 (w)	0 + 1235 + 472
33660 (w)	0 + 210	36177 (ms)	0 + 2 × 926
33705 (m)	0 + 256	36572 (m)	0 + 2 × 663 + 926
33789 (s)	0 + 340	36896 (w)	0 + 2 × 663 + 1235
33879 (m)	0 + 430	37098 (m)	0 + 3 × 926
33974 (vs)	0 + 525		
34044 (m)	0 + 2 × 340 — 85		
34125 (w)	0 + 2 × 340 0 + 256 + 430		
34260 (w)	0 + 811		
34316 (w)	0 + 340 + 525 0 + 2 × 430		
34332 (w)	0 + 210 + 676		
34437 (vw)	0 + 988		
34496 (m)	0 + 2 × 525		
34857 (w)	0 + 1408 0 + 2 × 515 + 340		
34942 (w)	0 + 2 × 340 + 811		

(i) $n \rightarrow \pi^*$ *Transitions* (*Transition I*)

The sharp band at 33449 cm^{-1} which persists with undiminished intensity even at the low pressure of the absorbing vapour has been taken as the 0, 0 band of this system. Most of the remaining strong bands represent transitions involving excited state vibration frequencies 210, 256, 340, 525, 811, 988 and 1408 cm^{-1} and also ground state frequencies 226, 292, 379, 455 and 564 cm^{-1} as shown in

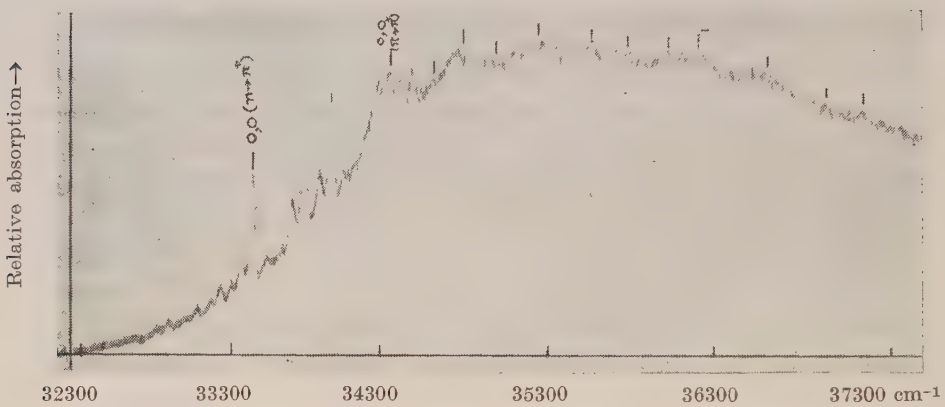

Fig. 1. Microphotometric record of the ultraviolet absorption spectrum of 2-aminopyridine in the vapour phase.

Table I. The bands of wave numbers higher than 34125 cm^{-1} are superposed on those due to $\pi \rightarrow \pi^*$ transition and this makes their accurate measurement somewhat uncertain. The band of medium strength at 33364 cm^{-1} is probably not due to a $v \rightarrow 0$ transition as no corresponding $0 \rightarrow v$ transition with greater strength could be detected. It was, therefore, assigned to a $v \rightarrow v'$ transition as shown in Table I. The weak band at a distance of 70 cm^{-1} from the 0, 0 band on the high energy side is also similarly assigned as a $v \rightarrow v'$ transition.

(ii) $\pi \rightarrow \pi^*$ *Transition* (*Transition II*)

The band system in the region 34300 cm^{-1} to 37200 cm^{-1} consisting of broad bands which are distinctly different from the sharp narrow bands due to the Transition I has been attributed to the $\pi \rightarrow \pi^*$ transition from their resemblance with the bands in the substituted benzene compounds.

It was difficult to find out the exact position of the 0, 0 band of this system because of the superposition of some bands due to $n \rightarrow \pi^*$ transition on these bands. However, the centre of the strongest broad band on the long wavelength side of of this system is at 34324 cm^{-1} and this has been taken as the position of the 0, 0 band. The other bands could then be assigned as progressions and combinations of excited state frequencies 294, 472, 663, 926, 1235 and 1441 cm^{-1}.

The infrared absorption spectrum above 990 cm^{-1} of this compound was earlier studied by Katritzky and Hands (1958) who reported the frequencies 991(ms)

Indian Journal of Physics, Vol. XXXV, No. 8

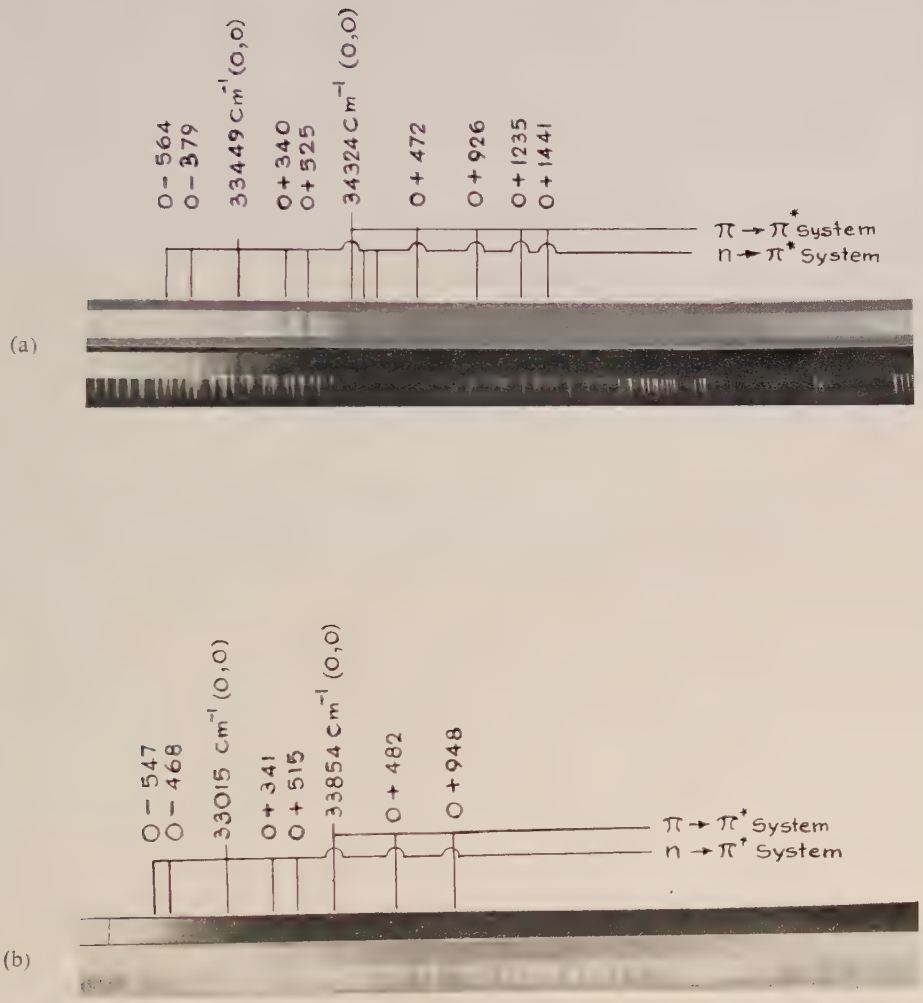

Fig. 4. Ultraviolet absorption spectra of aminopyridines in the vapour phase
(a) 2—Aminopyridine vapour.
(b) 3—Aminopyridine vapour.

TABLE II

Ultraviolet absorption bands of 2-aminepyridine ($\pi \rightarrow \pi^*$ systems)

.01% solution in alcohol at 32°C		.01% solution in *n*-hexane at 32°C	
Wave number (cm^{-1}) and strength	Assignment	Wave number (cm^{-1}) and strength	Assignment
Broad absorption band extending from 32414 cm^{-1} to 36000 cm^{-1} without any discrete structure		32885 (s)	0,0
		33363 (m)	0 + 478
		33830 (m)	0 + 945
		34317 (m)	0 + 1432
		34782 (m)	0 + 2 × 945
		35755 (m)	0 + 2 × 1432

1038 (m), 1148 (s), 1270 (ms), 1317 (s), 1441 (s), 1483 (vs), 1574 (s) and 1602 (vs), being the strengths of the bands are given in parentheses. The infrared spectrum of solution of 2-aminopyridine in CCl_4 was reinvestigated down to 600 cm^{-1} and besides the above frequencies a band at 710 cm^{-1} was observed.

The excited state frequencies 663cm^{-1}, 926 cm^{-1} and 1235 cm^{-1} evidently correspond respectively to the ground state frequencies 710 cm^{-1}, 991 cm^{-1} and 1270 cm^{-1} observed in the infrared spectra. Two ground state frequencies 1441 cm^{-1} and 1483 cm^{-1} have been reported by Katritzky and Hands (1958) and it may be noted that the band assigned to the excited state frequency 1441 cm^{-1} in the present investigation is quite broad and it may comprise two unresolved bands.

(b) *Influence of intermolecular field on the spectra*

(i) *Spectra of the solutions*

In the spectrum of solution of 2-aminopyridine in *n*-hexane (Fig. 2) a band system consisting of broad absorption bands is observed in the region 32500 cm^{-1}

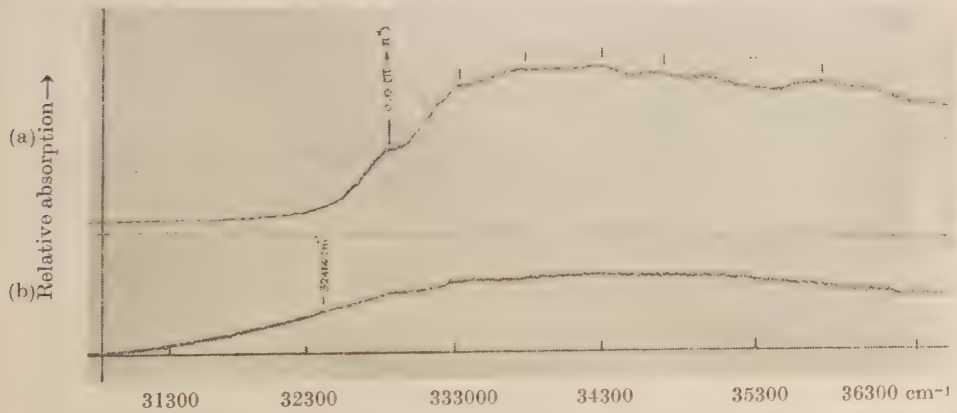

Fig. 2. Microphotometric records of the ultraviolet absorption spectra of solutions of 2-amino pyridine.

(a) .01% solution in *n*-hexane. b) .01% solution in ethyl alcohol.

to 36000 cm^{-1}. From the structure of this band system, it appears that this system corresponds to the $\pi \rightarrow \pi^*$ transition in the vapour phase. Taking the first strong band at 32885 cm^{-1} as the 0,0 band of this system, the other bands can be analysed in terms of the excited state frequencies 478 cm^{-1}, 945 cm^{-1} and 1432 cm^{-1} and their harmonics. Thus in the case of *n*-hexane solution this band system is shifted towards red by 1461 cm^{-1}. As the 0, 0 band in the $n \rightarrow \pi^*$ system due to the vapour is at 33449 cm^{-1} and the 0, 0 band of the $\pi \rightarrow \pi^*$ transition in solution of hexane is at 32885 cm^{-1} it is quite probable that the former system is masked by the strong system due to $\pi \rightarrow \pi^*$ transition.

In the spectrum of .01% solution of 2-aminopyridine in ethyl alcohol (Fig. 2) only one very broad band due to $\pi \rightarrow \pi^*$ transition is in the region 32000 cm^{-1} to 36000 cm^{-1}. If the 0, 0 band is assumed to be at about 32414 cm^{-1}, which is the long wavelength edge of the borad band the band system seems to be shifted towards red by about 1910 cm^{-1} from its position in the case of the vapour.

The appearance of the band system due to the solution in alcohol is different from that of the system due to the *n*-hexane solution and it is similar to that of the pure liquid. The shift of the system is also much larger than that observed in the case of the solution in hexane. These results probably indicate the formation of associated groups of 2-aminopyridine molecules with neighbouring alcohol molecules due to hydrogen bond-formation as suggested by Stephenson (1954) and Roy (1958) in the cases of other pyridine compounds.

(ii) *Spectra due to the substances in the liquid and solid states*

In the spectrum of 2-aminopyridine in the liquid state at 70°C a broad absorption band without any discrete structure is observed in the region from 32368

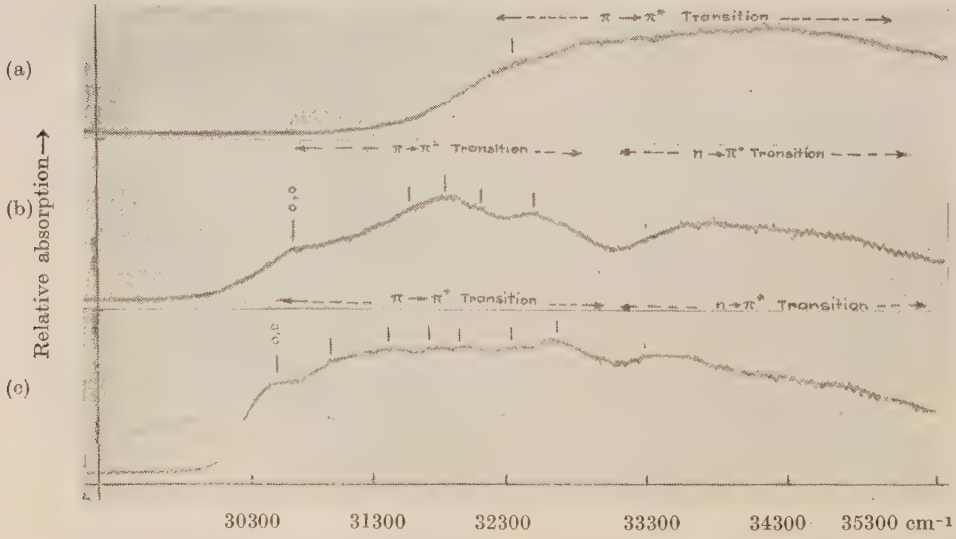

Fig. 3. Microphotometric records of the ultraviolet absorption spectra of 2-aminopyridine.
(a) Liquid at 70°C. (b) Solid at 33°C. (c) Solid at −180°C.

cm^{-1} to 35421 cm^{-1}. This absroption appears to be due to the $\pi \rightarrow \pi^*$ transition. If we assume that the 0, 0 band of this transition lies near about the hump at 32368 cm^{-1} on the long wavelength edge of the system, the 0, 0 band seems to be displaced towards red by about 2440 cm^{-1} on liquefaction of the vapour.

This shift of the band system and the absence of discrete structure of the system may be due to formation of associated groups among neighbouring molecules. On comparing these results with those for the solution in alcohol it is found that the nature of association in the two cases is different, because the shift of the band system is much larger in the case of the pure liquid than in the solution in alcohol.

TABLE III

Ultraviolet absorption bands of 2-aminopyridine in the liquid and solid states

System	Liquid at 70°C		Solid at 32°C		Solid at —180°C	
	Wave number (cm^{-1}) and strength	Assignment	Wave number (cm^{-1}) and strength	Assignment	Wave number (cm^{-1}) and strength	Assignment
Transition II	Broad absorption extending from 32368 cm^{-1} to 35421 cm^{-1}		30684 (m)	0,0	30497 (s)	0,0
			31611 (m)	0 + 927	30968 (m)	0 + 471
			31929 (s)	0 + 1245	31430 (m)	0 + 933
			32134 (m)	0 + 1450	31746 (m)	0 + 1249
			32535 (m)	0 + 2×927	31964 (m)	0 + 1467
					31357 (m)	0 + 2×933
					32680 (ms)	0 + 933 + 1249
Transition I	Not observed		Board band in the region 33300 cm^{-1} —35000 cm^{-1}		Board band in the region 33300 cm^{-1} —35000 cm^{-1}	

When the liquid is solidified at room temperature discrete band structure is observed, but the spectrum seems to be somewhat different from that due to the vapour phase. Not only the band system due to the solid is shifted towards red but also the individual bands are much broader so that they are not resolved clearly. This may be due to small splitting caused by the influence of the neighbouring polar molecules in the crystal on the transition moment. Taking the 0, 0 band to be at 30684 cm^{-1} the excited state frequencies 927 cm^{-1}, 1245 cm^{-1} and 1450 cm^{-1} may be attributed to the other bands. It also appears that the spectrum consists of two parts, the second part starting from about 33200 cm^{-1} and extending upto about 35000 cm^{-1}. As the 0, 0 band of the $n \rightarrow \pi^*$ system of the vapour is at 33449 cm^{-1} probably this second portion of the spectrum due to the substance in the solid state is produced by the $n \rightarrow \pi^*$ transition. The bands due to $n \rightarrow \pi^*$ transition are too broad to be resolved from each other probably

because of the same reason as indicated above. Thus it appears that in this case the $n \rightarrow \pi^*$ transition persists in the solid state. In the spectrum due to the liquid also, this second part seems to be superposed on the first part but the shift of the first part being smaller than that in the case of the solid the two parts are not separated from each other.

When the solid is cooled to $-180°C$, the bands are found to remain broad and the absorption becomes stronger. The strong band at 30497 cm^{-1} has been taken as the 0,0 band and the upper state fundamentals 471, 933, 1249 and 1467 cm^{-1} have been observed, as shown in Table III. The second part due to $n \rightarrow \pi^*$ transition seems to persist at $-180°C$ in the same position as at the room temperature.

As the $n \rightarrow \pi^*$ transition seems to persist in this solid state also, it seems that the nitrogen atom of the ring does not take part in weak bond-formation. It is quite probable that the NH_2 group is responsible for hydrogen bond-formation with the neighbouring molecules and in that case the effect is expected to be similar to that of the substitution of a hydrogen atom of the ring and consequently a shift of the band system towards red is expected. In the case of the solid at the room temperature the shift is about 3740 cm^{-1} from its position in the case of the vapour, while with further cooling to $-180°C$, the 0, 0 band experiences a further shift of 187 cm^{-1} towards red. The large shift of the 0, 0 band on solidification of the liquid and very small shift with further cooling and also the small splitting to which the broadening of the bands were attributed may be due tothe influence of intermolecular field in the crystal on the electronic energy levels of the molecule.

3-*Aminopyridine*

Microphotometric records of the absorption spectra of 3-aminopyridine in different states and in solutions in different solvents are reproduced in Figs. 5-7 and the spectrum of the substance in the vapour phase is reproduced in Plate IX, Fig. 4(b). Wave numbers of the bands in cm^{-1}, their approximate strengths and their probable assignments are given in Table IV-VI.

(a) *Spectrum due to the vapour phase*

The absorption spectrum of 3-aminopyridine in the vapour phase shows two distinct systems of bands as shown in Fig. 5. In the case of the vapour at the saturation pressure at 60°C and with a path length of 50 cm a system consisting of sharp, narrow bands appears on the long wavelength side of another system consisting of broad bands. As in the case of 2-aminopyridine, the former system has been attributed to the $n \rightarrow \pi^*$ transition and the latter to the $\pi \rightarrow \pi^*$ transition.

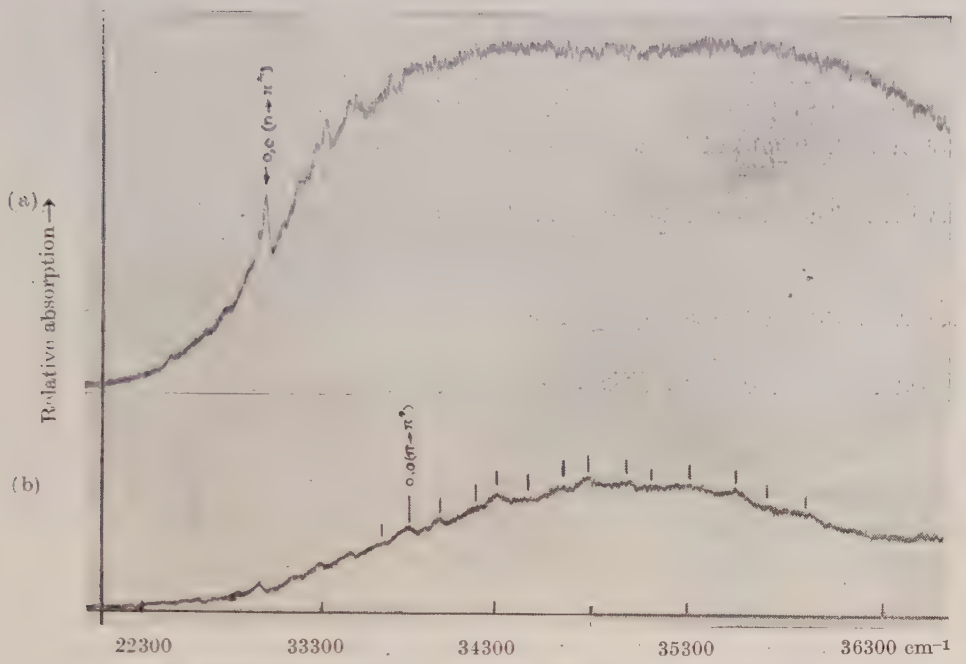

Fig. 5. Microphotometric records of the ultraviolet absorption specctra of 3-aminopyridine in the vapour phase.
(a) $n \rightarrow \pi^*$ transition. (b) $\pi \rightarrow \pi^*$ transition.

TABLE IV

Ultraviolet absorption bands of 3-aminopyridine in the vapour phase

Transition I		Ttransition II	
Wave number (cm^{-1}) and strength	Assignment	Wave number (cm^{-1}) and strength	Assignment
32462 (w)	0 — 547	33690 (m)	0 — 164
32547 (w)	0 — 468	33854 (s)	0,0
32691 (w)	0 — 324	34004 (ms)	0 + 150
32777 (m)	0 — 238	34208 (m)	0 + 354
32891 (w)	0 — 124	34336 (s)	0 + 482
32961 (w)	0 + 181 — 238	34494 (w)	0 + 640
33015 (vs)	0,0	34712 (m)	0 + 858
33119 (m)	0 + 104	34802 (s)	0 + 948
33196 (m)	0 + 181	35009 (m)	0 + 1160 0 + 2 × 150 + 858
33301 (m)	0 + 270	35128 (m)	0 + 1274 0 + 2 × 640
33356 (s)	0 + 341		
33520 (m)	0 + 515	35353 (m)	0 + 1499 0 + 858 + 640
		35579 (w)	0 + 2 × 858
		35754 (w)	0 + 2 × 948
		35918 (w)	0 + 150 + 2 × 948

(i) *$n \rightarrow \pi^*$ transition (Transition I)*

The bands due to $n \rightarrow \pi^*$ transition in 3-aminopyridine lie in the region 32300 cm^{-1} to 33800 cm^{-1}. The sharp and strong band at 33015 cm^{-1} has been taken as the 0, 0 band of the system the other bands have been analysed in terms of upper state fundamentals 104, 181, 270, 341 and 515 cm^{-1} and their combinations. The corresponding ground state vibrational wave numbers as obtained from $v \rightarrow 0$ transitions are probably 124, 238, 324, 468 and 547 cm^{-1}.

It may be noted for comparison that the excited state variational wave numbers 131 cm^{-1}, 158 cm^{-1}, 264 cm^{-1} 499 cm^{-1}, 545 cm^{-1} and 580 cm^{-1} were reported by Rush and Sponer (1952) in the case of $n \rightarrow \pi^*$ transition in 3-methyl pyridine and in the case of 3-bromopyridine the corresponding wave numbers were found to be 230 cm^{-1}, 279 cm^{-1}, 349 cm^{-1} and 579 cm^{-1} (Misra, 1960).

The band at 32961 cm^{-1} on the longer wavelength side of the 0, 0 band has been assigned as a $v \rightarrow v'$ transition. The assignments of the bands on the high energy side of the system is somewhat uncertain due to overlapping of the bands due to $n \rightarrow \pi^*$ transition with those due to $\pi \rightarrow \pi^*$ transition.

(ii) *$\pi \rightarrow \pi^*$ transitions (Transition II)*

The band system due to $\pi \rightarrow \pi^*$ transition in 3-aminopyridine in the vapour phase lies in the region from 33600 cm^{-1} to 36500 cm^{-1}. As in the case of 2-aminopyridine there is some uncertainty in locating exactly the 0, 0 band of this system due to the overlapping of the two transitions in this region, as stated in the previous section. However, the strong band on the long wavelength side of this system at 33854 cm^{-1} whereform the broad absorption system seems to start at higher pressure of the absorbing vapour is taken tentatively as the 0, 0 band. Most of the remaining bands represent transitions involving excited state vibrational frequencies 150, 354, 482, 640, 858, 948, 1160, 1274 and 1499 cm^{-1} as shown in Table IV. Moreover, a ground state frequency 164 cm^{-1} is observed as $v \rightarrow 0$ transition. In order to find out the ground state vibrational frequencies, the infrared absorption spectrum of 3-aminopyridine in chloroform solution was studied with a Perkin Elmer Model 21 spectrophotometer with NaCl optics. The wave numbers of some of the observed infrared bands are 690 (m), 790 (m), 885 (m), 1013(s), 1042(s), 1090 (w), 1220 (w), 1255 (m), 1285 (s), 1438 (vs), 1485 (s), 1580 (vs) cm^{-1}, the strength of absorption being given in the paretheses. The infrared frequencies 690 cm^{-1} and 885 cm^{-1} may correspond to the excited state frequencies 640 cm^{-1} and 858 cm^{-1} observed in the ultraviolet absorption spectrum. There are two medium strong infrared absorption bands of ground state frequencies 1013 cm^{-1} and 1042 cm^{-1} but only one excited state frequency 948 cm^{-1} is observed in the ultraviolet absorption spectrum. The bands at a distance of 1160 cm^{-1}, 1274 cm^{-1} and 1499 cm^{-1} from the 0, 0 band shown as combinations, may also be fundamentals as there are strong bands with vibrational frequencies 1220 cm^{-1}, 1285 cm^{-1} and 1580 cm^{-1} in the infrared spectrum.

(b) *Influence of intermolecular field on the spectra*

(i) *Spectra due to the solutions*

In the spectrum of 3-aminopyridine in *n*-hexane solution broad absorption bands corresponding to those due to the $\pi \rightarrow \pi^*$ transition in the vapour phase

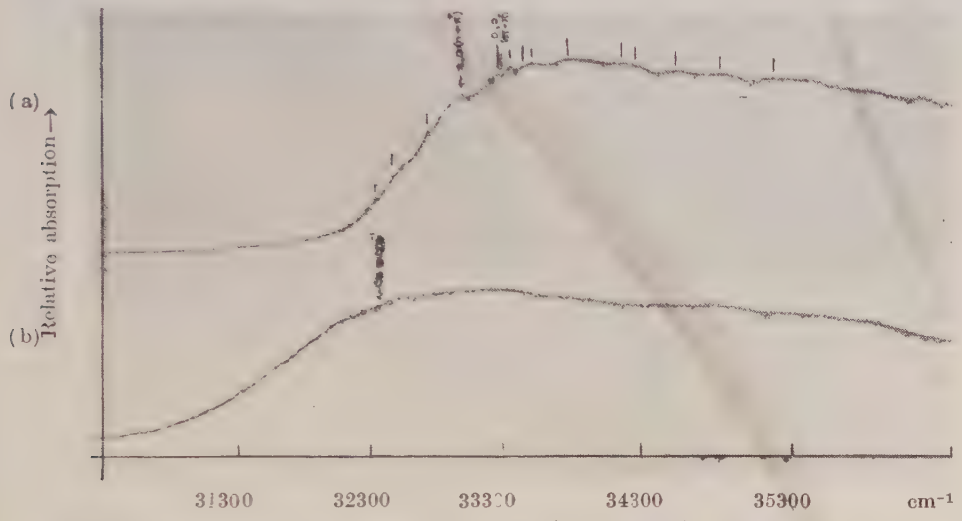

Fig. 6. Microphotometric record of the ultraviolet absorption spectra of solutions of 3-aminopyridine.

(a) .01% solution in *n*-hexane. (b) .01% solution in ethyl alcohol.

TABLE V

Ultraviolet absorption bands of 3-aminopyridine in solution

System	Solution in alcohol at 32°C		Solution in *n*-hexane at 32°C	
	Wave number (cm^{-1}) and strength	Assignment	Wave number (cm^{-1}) and strength	Assignment
Transition II	Broad absorption band extending from 31437 cm^{-1} to 35857 cm^{-1}		33301 (s)	0,0
			33461 (m)	0 + 160
			33779 (m)	0 + 478
			34154 (m)	0 + 853
			34248 (m)	0 + 947
			34473 (m)	0 + 1173
			34784 (m)	0 + 1483
			35200 (m)	0 + 2 × 947
Transition I	Absent		32472 (w)	0 — 543
			32776 (w)	0 — 239
			33015 (s)	0,0
			33357 (w)	0 + 342
			33524 (m)	0 + 509

are observed. Assuming the broad band at 33301 cm^{-1} as the 0, 0 band of the system, the other bands can be explained in terms of excited state frequencies 160, 478, 853, 947, 1173, 1483 cm^{-1} and their combinations as shown in Table V. These upper state fundamentals agree fairly well with those observed in the spectrum due to the vapour.

In addition to the above broad bands a few sharp weak bands are also observed in the spectrum of 3-aminopyridine in *n*-hexane solution at 33015, 32776 and 32468 cm^{-1}. There are also two weak bands at 33357 cm^{-1} and 33520 cm^{-1}. The positions of these bands are found to be indentical with those of bands of $n \rightarrow \pi^*$ system due to the vapour phase and therefore the $n \rightarrow \pi^*$ system persists in the solution in *n*-hexane. So, the $n \rightarrow \pi^*$ transition is not affected appreciably by the solvent molecules.

In alcohol solution, however, no banded structure is observed and only a very broad absorption band extending from 31437 cm^{-1} to 35857 cm^{-1} is observed. As in the case of 2-amino isomer, this absorption seems to correspond to the $\pi \rightarrow \pi^*$ transition. The absorption increases rapidly and becomes large at 32321 cm^{-1}. So, the system seems to be shifted by about 1500 cm^{-1} towards red from its position in the spectrum due to the vapour. The position of the system due to the $n \rightarrow \pi^*$ transition is almost at the maximum of the broad band. So it is not possible to come to any conclusion regarding the appearance or otherwise of this system in case of the solution in alcohol.

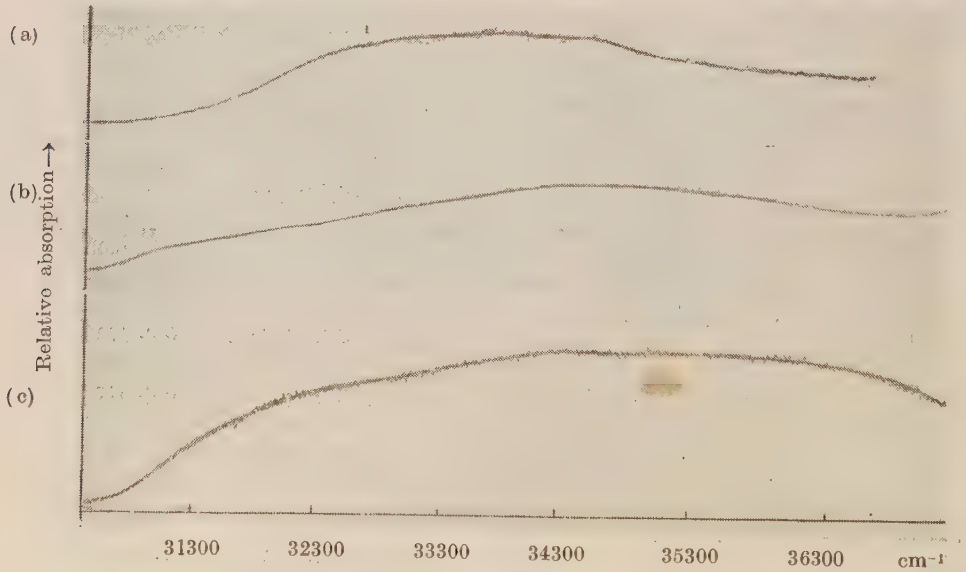

Fig. 7. Microphotometric records of the ultraviolet absorption spectra of 3-aminopyridine

(a) Liquid at 70°C. (b) Solid at 32°C. (c) Solid at −180°C.

(ii) *Spectra in the liquid and solid states*

In the liquid state 3-aminopyridine shows only a very broad absorption band without any discrete structure in the region 31650 cm^{-1} to 35450 cm^{-1} as shown in Fig. 7. The appearance is similar to that due to the solution in alcohol. In this case also nothing can be said about the presence or absence of the system due to the $n \rightarrow \pi^*$ transition.

TABLE VI

Ultraviolet absorption bands of 3-aminopyridine in the liquid and solid states

Liquid at 70°C	Solid at 32°C	Solid at —180°C
Broad absorption band extending from 31650 cm^{-1} to 35450 cm^{-1}	Broad absorption band extending from 30760 cm^{-1} to 36780 cm^{-1}	Broad absorption band extending from 30760 cm^{-1} to 36780 cm^{-1}

When the substance is solidified at the room temperature no discrete structure of the band system is observed but the region of absorption becomes extended on both sides. When the substance is further cooled to—180°C, no further appreciable change in the spectrum takes place. It is interesting, however, that in this case the width of the region of absorption is about 6000 cm^{-1}. This is double the breadth of the $\pi \rightarrow \pi^*$ system due to the vapour phase. This increase in the width of the region may be due to the large unresolved splitting of the system caused by the intermolecular field in the crystal lattice.

ACKNOWLEDGMENT

The author is indetbed to Professor S. C. Sirkar, D.Sc., F.N.I., for his kind interest and guidance in the work. Thanks are also due to Dr. S. B. Banerjee for many helpful discussions.

REFERENCES

Banerjee, S. B., 1956, *Ind. J. Phys.*, **30**, 480.
Banerjee, S. B., 1957, *Ind. J. Phys.*, **31**, 11.
Kasha, M., 1950, Discussion of the Faraday Society No. **9**, 14.
Katritzky, A. R., and Hands, A. R., 1958, *J. Chem. Soc.*, Part II, p. 2202.
Misra, T. N., 1960, *Ind. J. Phys.*, **34**, 381.
Roy, S. B., 1958, *Ind. J. Phys.*, **32**. 323.
Rush, J. H. and Sponer, H., 1952, *J. Chem. Phys.*, **20**, 1847.
Sirkar, S. C. and Misra, T. N., 1959, *Ind. J. Phys.*, **33**, 45.
Stephenson, H. P., 1954, *J. Chem. Phys.*, **22**, 1077.

Letters to the Editor

The Board of Editors will not hold itself responsible for opinions expressed in the letters published in this section. The notes containing reports of new work communicated for this section should not contain many figures and should not exceed 500 words in length. The contributions must reach the Assistant Editor not later than the 15th of the second month preceding that of the issue in which the letter is to appear. No proof will be sent to the authors.

5

ON THE EVALUATION OF THE COEFFICIENTS OF THERMAL EXPANSION OF CRYSTALS FROM X-RAY DATA

V. T. DESHPANDE AND V. M. MUDHOLKER

DEPARTMENT OF PHYSICS, UNIVERSITY COLLEGE OF SCIENCE,
OSMANIA UNIVERSITY, HYDERABAD-7.

(*Received December* 6, 1960)

The purpose of this note is to call attention to some small but vital differences obtained in the methods used in processing X-ray data for the evaluation of the coefficients of thermal expansion. In view of the increased importance of this property of crystalline solids in relation to their structural imperfections, it has become necessary to know, not merely the average values of the coefficient of expansion but also the temperature dependence of the instantaneous values. It is essential, therefore, that the methods used in processing the X-ray data be chosen in a way so as to bring out the correct form of this temperature variation. It is, of course, assumed that the data on cell dimensions are obtained with the highest possible accuracy, taking care to correct all errors, systematic or random.

An important step in this processing is the determination of the derivative (da/dt) at different temperatures. This, with the help of the definition, $\alpha = (1/a_0)(da/dt)$, gives the values of the zero coefficient of expansion at those temperatures. Different methods are in use for the evaluation of this derivative. One of these, used by Wilson (1941), is to obtain the mean value of the derivative over small intervals of temperature by subtracting the experimental values of 'a' and dividing these by the corresponding temperature differences. A variation of this procedure, employed by some workers (Owen and Richards, 1936 and Deshpande and Mudholker, 1960) consists in obtaining the mean values of the derivative from a carefully drawn graph between 'a' and 't'. The values of 'α' are then evaluated for every temperature at which the derivative is found. Least squares treatment of the α-t data, thus obtained, then gives the temperature

dependence of 'α'. This dependence may or may not be linear, a fact which comes out readily from the α-t plot. If the relation is non-linear it is usually expressed in the form given in Eq. (1).

$$\alpha = \alpha_0 + \beta t + \gamma t^2 \qquad \ldots \quad (1)$$

In another method (Stokes and Wilson, 1941 ; Kempter and Elliot, 1959 ; Pathak and Pandya, 1960 and Pathak and Pandya, 1960a) the lattice constant is first expressed as quadratic function of temperature, by the usual method of least squares, giving an expression, as in Eq. (2).

$$a = a_0 + bt + ct^2 \qquad \ldots \quad (2)$$

Differentiation of Eq. (2) with respect to temperature, then, gives the coefficient of expansion as a linear function of temperature as shown in Eq. (3)

$$\alpha = \alpha_0 + \beta t \qquad \ldots \quad (3)$$

This procedure appears to be more rigorous than the first one, but has a serious limitation in as much as the temperature dependence of 'a' comes out necessarily to be linear. This may or may not be its real form. Wilson (1941) has found that this method does not give the best possible representation of the derivative (da/dt), and Stokes and Wilson (1941) have pointed out that in principle, the quadratic function is not satisfactory.

There is thus a fundamental difference between the two methods outlined above. While the first method brings out the non-linear character of the $\alpha - t$ relation, the second one supresses it. This limitation in the second method can be removed if a cubic function in 't' is used instead of Eq. (2). Owen and Williams (1954) have given such an expression for the lattice constant of silver. Similar procedure has also been used by Dheer and Surange (1958) in their macroscopic study on lead. However, this procedure is rarely followed, perhaps because of the larger amount of computational work involved in it.

As a sample case, we have processed the X-ray data on sodium chlorate (Deshpande and Mudholker 1960) by all these method, The results are shown in Fig. 1. Curves I and II represent the results of the first two methods respectively and curve III is obtained by the use of the cubic expression. It is clear from the that there is a close agreement between the curves I and III. Curve II not only suppresses the non-linear variation of 'α' with 't' but, in this particular case, there are significant differences in the values of 'α' at some temperatures. For other substances the values of 'α' given by the three methods may agree with each other, within certain limits, but the possible non-linear nature of $\alpha - t$ curve can not be brought by the second method. The amount of calculations involved in the third method makes it rather lengthy and hence, the first method seems

to offer a practicable procedure for obtaining dependable results on the temperature variation of the coefficient of thermal expansion.

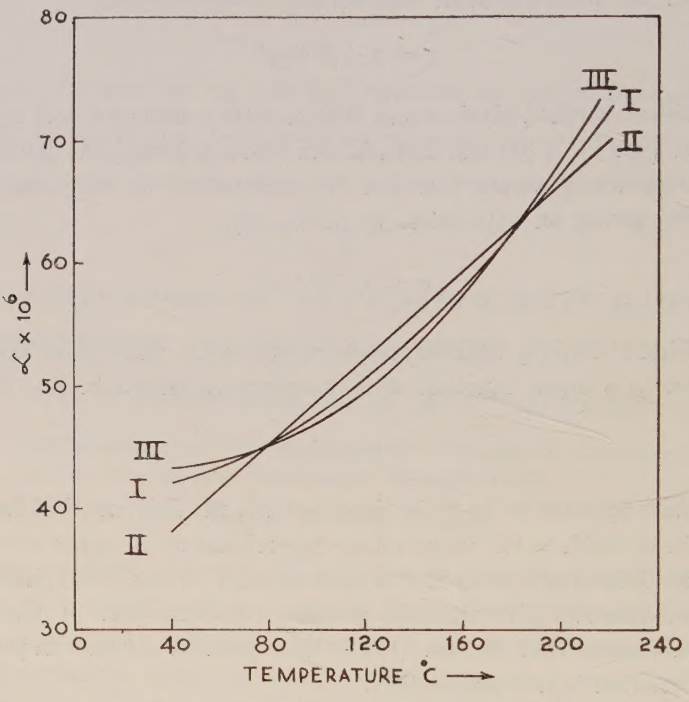

Fig. 1. 'α' vs 't' plots for sodium chlorate as obtained by the three methods of processing X-ray data.

One of the authors, (V.M.M.) is grateful to the Council of Scientific and Industrial Research for the award of a Junior Research Fellowship.

REFERENCES

Deshpande, V. T. and Mudholker, V. M., 1960, *Acta Cryst.*, **13**, 482.

Dheer, P. N. and Surange, S. L., 1958, Low Temperature Physics and Chemistry, p. 592, Edited by Dillinger, The University of Wisconsin Press.

Kempter, C. P. and Elliot, R. O., 1959, *J. Chem. Phys.*, **30**, 1524.

Owen, E. O. and Richards, T. Ll., 1936, *Phil. Mag.* **22**, 304.

Owen, E. O. and Williams, G. I., 1954, *J. Sci. Instr.*, **31**, 49.

Pathak, P. D. and Pandya, N. V., 1960, *Current Science*, **29**, 14.

Pathak, P. D. and Pandya, N. V., 1960 a, *Ind. J. Phys.* **34**, 416.

Stokes, A. R. and Wilson. A. J. C., 1941, *Proc. Phys. Soc.* **53**, 658.

Wilson, A. J. C., 1941, *Proc. Phys. Soc.* **53**, 235.

IMPORTANT PUBLICATIONS

The following special publications of the Indian Association for the Cultivation of Science, Jadavpur, Calcutta, are available at the prices shown against each of them:—

TITLE	AUTHOR	PRICE
Magnetism ... Report of the Symposium on Magnetism		Rs. 7 0 0
Iron Ores of India	... Dr. M. S. Krishnan	5 0 0
Earthquakes in the Himalayan Region	... Dr. S. K. Banerji	3 0 0
Methods in Scientific Research	.. Sir E. J. Russell	0 6 0
The Origin of the Planets	.. Sir James H. Jeans	0 6 0
Active Nitrogen—A New Theory.	.. Prof. S. K. Mitra	2 8 0
Theory of Valency and the Structure of Chemical Compounds.	.. Prof. P. Ray	3 0 0
Petroleum Resources of India	.. D. N. Wadia	2 8 0
The Role of the Electrical Double-layer in the Electro-Chemistry of Colloids.	.. J. N. Mukherjee	1 12 0
The Earth's Magnetism and its Changes	.. Prof. S. Chapman	1 0 0
Distribution of Anthocyanins	.. Robert Robinson	1 4 0
Lapinone, A New Antimalarial	.. Louis F. Fieser	1 0 0
Catalysts in Polymerization Reactions	.. H. Mark	1 8 0
Constitutional Problems Concerning Vat Dyes.	.. Dr. K. Venkataraman	1 0 0
Non-Aqueous Titration	.. Santi R. Palit, Mihir Nath Das and G. R. Somayajulu	3 0 0
Garnets and their Role in Nature	.. Sir Lewis L. Fermor	2 8 0

A discount of 25% is allowed to Booksellers and Agents.

NOTICE

No claims will be allowed for copies of journal lost in the mail or otherwise unless such claims are received within 4 months of the date of issue.

RATES OF ADVERTISEMENTS

1. Ordinary pages:
   - Full page .. .. Rs. 50/- per insertion
   - Half page .. .. Rs. 28/- per insertion
2. Pages facing 1st inside cover, 2nd inside cover and first and last page of book matter:
   - Full page .. .. Rs. 55/- per insertion
   - Half page .. .. Rs. 30/- per insertion
3. Cover pages .. .. by negotiation

25% commissions are allowed to *bona fide* publicity agents securing orders for advertisements.

CONTENTS

Indian Journal of Physics Vol. 35, No. 8 August, 1961

PRINTED BY KALIPADA MUKHERJEE, EKA PRESS, 204/1, B. T. ROAD, CALCUTTA-35
PUBLISHED BY THE REGISTRAR, INDIAN ASSOCIATION FOR THE CULTIVATION OF SCIENCE
2 & 3, LADY WILLINGDON ROAD, CALCUTTA-32